Fabrication and Performance Analysis of Fe_2O_3 Doped TiO_2 Dye Sensitized Solar Cell

M.S. THESIS

Institute of Energy

University of Dhaka

A thesis on

Fabrication and Performance Analysis of Fe_2O_3 Doped TiO_2 Dye Sensitized Solar Cell

A thesis is submitted to the Institute of Energy at theUniversity of Dhaka in partial fulfillment of the requirementsfor the Degree of Masters of Science in Renewable Energy Technology

By

ShafiulAzam

3rdBatch, Roll: 34, Registration: HA-319

Session: 2013-2014

Dedication

To

Teacher and the source of human knowledge of our

Prophet Muhammad (peace be upon him)

To

Like fatherhood Highest ... And my dear father

To

granule my heart first ... my mother compassionate

Abstract

Solar energy is a renewable free source of energy that is sustainable and totally inexhaustible, unlike fossil fuels which are finite. Solar power is clean green electricity that is either created from sunlight or from heat from the sun. Solar (or photovoltaic) cells convert the sun's energy into electricity. Whether they're adorning your calculator or orbiting our planet on satellites, they rely on the photoelectric effect: the ability of matter to emit electrons when a light is shone on it. As the name implies, the mechanism of dye solar cells is based on the photo electrochemical processes. This paper aims to fabricate and analyze the performance of dye sensitized solar cell by comparing the utilization of opaque TiO_2 pastes and opaque TiO_2 pastes with Fe_2O_3 doping for the photoelectrodes. Among other semiconductors, hematite (Fe_2O_3) is an attractive material because of its wide abundant, low cost, non-toxic nature. It is gaining importance in photo-electrochemical devices due to its suitable band gap (~2.2 eV). It has been reported that the use of nanostructured materials in the DSSC could enhance the low energy conversion efficiency of these cells. The current-voltage (I-V) measurements were performed by using an artificial sun-simulator. As for the counter-electrode, carbon (C) was used as the catalyst which was deposited using DC-sputtering technique. Our results revealed that the cells featuring opaqueTiO_2 paste with Fe_2O_3 doping achieved better photoconversion efficiencies compared to that of the opaque TiO_2 paste. This combination further increases its optical transmittance and band gap of the photo electrode of DSSC. The sole purpose was to optimize the characteristics of this material by focusing on its several characteristics followed by changing the duration of solution preparation, changing the deposition level on substrates, variation in annealing atmosphere and temperature to observe the characteristics changes occurred in the film. In each stage of observation significant characteristics of the film have found which the main execution of this thesis.

Table of Contents

List of Figures

List of Tables

1 Chapter 1

1.1 Introduction

In the modern world of technological advancements, energy has become one of the basic needs for life. With the increase in world population, so is rising the energy demand. The worldwide power consumption is expected to double in the next 3 decades, and the limited supply of fossil fuels is hardly expected to cope with this. Nuclear power, though capable of providing large scale power generation, is being proven to be guilty in safety and waste management issues. Hence, sooner or later we need to turn to renewable energy sources, and the most viable candidate of them is solar energy.

Among all other abundant and non-polluting renewable energy sources (examples include solar, wind, water and geothermal heat) in our planet, solar energy is expected to play a vital role as a future energy source. We receive about 3×1024 joule/year energy in the form of sunlight to the earth's surface, which is nearly 104 times more than the world's energy consumption.1While the sun can provide, we are in need of devising practical approach for conversion, storage and distribution of this energy.

Alternative energy is a term used to refer to any energy source other than fossil fuels. An ongoing debate exists over what forms of alternative energy are the safest, most cost-efficient, and most practical to replace and/or subsidize fossil fuels. Some activists believe that government agencies and powerful lobbyists are hindering investigation into alternative energy in an effort to support the fossil fuel industry. As a source of energy, fossil fuels are limited and cause numerous harmful environmental effects. Many modern energy companies are studying and developing alternative fuel sources. In recent years, governments have increased the resources dedicated to the developmentof alternative energy.

Climate change and the consumption of non-renewable resources are considered as the greatest problems facing humankind. Because of this, photocatalysis research has been rapidly expanding. TiO_2 nanoparticles have been extensively investigated for

photocatalytic applications including the decomposition of organic compounds and production of H_2 as a fuel using solar energy. TiO_2 is considered close to an ideal semiconductor for photocatalysis but possesses certain limitations such as poor absorption of visible radiation and rapid recombination of photogenerated electron/hole pairs.

Solar energy is one of the most popular renewable and sustainable energy resources. Among the different photovoltaic (PV) cells, dye-sensitized solar cells (DSSC) are promising candidate for renewable energy sources compared to silicon based solar cells. Although silicon based solar cells have high performance and good stability, but expensive fabrication cost limits its wideapplications as affordable device [101,102]. Compared to the conventional silicon-based solar cells, DSSC have many advantages such as low production cost, light weight, low environmental impact during fabrication, and applicability on flexible substrates [103,104]. In general, DSSC are composed of three active components such as semiconducting film, sensitizer, and redox electrolyte. In a typical DSSC, photogeneration of charge carriers occurs through light absorption by sensitizer, followed by a rapid charge separation. The electrons are injected into the semiconducting film while the separated holes are transported to counter electrode by means of redox process [105]. The ruthenium complexes have been mostly used as sensitizers and titanium oxide as semiconductor in DSSC.

Chou et al. [106] have used microcrystalline titanium oxide (TiO_2) for fabrication of DSSC. The effect of the average size of TiO_2 particles synthesized by the sol–gel method on the power conversion efficiency of a DSSC was reported. Lee et al. [107] have prepared a DSSC with a light scattering layer of 123 nm TiO_2 paste, and its overall power conversion efficiency of the DSSC device was achieved by 6.03%. Zinc oxide (ZnO) has been used as an alternative to TiO_2 for fabrication of DSSC [108]. The adsorption of cisrutheniumbis[2,20–bipyridine]-bis[4–thiopyridine] onto ZnOnanorods has been studied. Kahlout [109] has used nanostructured ZnO for fabrication of DSSC. The influence of the electrolyte iodine concentration, the film thickness, and the light intensity on the current density of the solar cell was studied.

Among other semiconductors, hematite (Fe_2O_3) is an attractive material because of its wide abundant, low cost, non-toxic nature. It is gaining importance in photo-electrochemical devices due to its suitable band gap (~2.2 eV) [110]. It has been reported

that the use of nanostructured materials in the DSSC could enhance the low energy conversion efficiency of these cells [111]. In this work, we report hydrothermal synthesis and application of nanostructured TiO_2 and Fe_2O_3 doped TiO_2semiconductor in DSSC. The effect of different light intensity on the current–voltage (I–V) characteristics of natural dye synthesized Fe_2O_3 based solar cell was studied.

2 Chapter 2

2.1 Renewable Energy

2.1.1 Renewable Energy as Alternative Source

Renewable energy is generally defined as energy that comes from resources which are naturally replenished on a human timescale, such as sunlight, wind, rain, tides, waves, and geothermal heat. Renewable energy replaces conventional fuels in four distinct areas: electricity generation, air and water heating/cooling, motor fuels, and rural (off-grid) energy services.

Renewable energy resources exist over wide geographical areas, in contrast to other energy sources, which are concentrated in a limited number of countries. Rapid deployment of renewable energy and energy efficiency is resulting in significant energy security, climate change mitigation, and economic benefits. In international public opinion surveys there is strong support for promoting renewable sources such as solar power and wind power. At the national level, at least 30 nations around the world already have renewable energy contributing more than 20 percent of energy supply. National renewable energy markets are projected to continue to grow strongly in the coming decade and beyond. Some places and at least two countries, Iceland and Norway generate all their electricity using renewable energy already, and many other countries have the set a goal to reach 100% renewable energy in the future. For example in Denmark the government decided to switch the total energy supply (electricity, mobility and heating/cooling) to 100% renewable energy by 2050. While many renewable energy projects are large-scale, renewable technologies are also suited to rural and remote areas and developing countries, where energy is often crucial in human development.

Renewable energy is reliable and plentiful and will potentially be very cheap once technology and infrastructure improve. It includes solar, wind, geothermal, hydropower and tidal energy, plus biofuels that are grown and harvested without fossil fuels. Nonrenewable energy, such as coal and petroleum, require costly explorations and potentially dangerous mining and drilling, and they will become more expensive as supplies dwindle and demand increases. Renewable energy produces only minute levels of carbon emissions and therefore helps combat climate change caused by fossil fuel usage. Renewable energy sources are so named because, aside from geothermal and tidal energies, they are replenished constantly by sunlight. Uneven solar heating of the Earth's surface causes wind. Sunlight also fuels the water cycle, which is harnessed through hydropower, including hydroelectric dams and less invasive systems that harness streams or ocean currents. Biofuels are grown using sunlight. Geothermal energy is considered renewable because radioactive decay in the Earth's core, which isn't expected to cool down any time soon, produces it. The gravitational pull of the sun and moon causes the tides.

Coal, natural gas and oil reserves are finite and hidden. An unknown and limited amount of each resource is buried deep underground or under the ocean. As more is harvested, finding new sources becomes more difficult and more expensive, and exploiting them becomes more challenging and sometimes dangerous as well. Marginal reserves, such as oil sands, require the burning of huge amounts of natural gas to refine them into usable oil. Drilling under the ocean floor can lead to catastrophic accidents, such as the British Petroleum oil spill of 2010. Renewable energy, by contrast, is as easy to find as wind or sunlight.

The daily price of oil depends on many factors, including political stability in historically volatile regions. Political strife has caused energy crises, including those that occurred in 1973 and 1979. Renewable energy can be locally produced and therefore is not vulnerable to distant political upheavals. Many of the safety concerns surrounding fossil fuels, such as explosions on oil platforms and collapsing coal mines do not exist with renewable energy.

Renewable energy is far cleaner than fossil fuels. Coal mining and petroleum exploration and refinement produce solid toxic wastes, such as mercury and other heavy metals. The

burning of coal to produce electricity uses large quantities of water often discharges arsenic and lead into surface waters and releases carbon dioxide, sulfur dioxide, nitrogen oxides and mercury into the air (see References 4). Gasoline and other petroleum products cause similar pollution. These pollutants cause respiratory illnesses and death in humans, produce acid rain that damages buildings and destroys fragile ecosystems, and deplete the ozone layer.

2.2 Major Renewable Energy Sources

2.2.1 Solar Energy

Solar energy, radiant light and heat from the sun, is harnessed using a range of ever-evolving technologies such as solar heating, photovoltaics, concentrated solar power, solar architecture and artificial photosynthesis. Solar technologies are broadly characterized as either passive solar or active solar depending on the way they capture, convert and distribute solar energy. Passive solar techniques include orienting a building to the Sun, selecting materials with favorable thermal mass or light dispersing properties, and designing spaces that naturally circulate air. Active solar technologies encompass solar thermal energy, using solar collectors for heating, and solar power, converting sunlight into electricity either directly using photovoltaics (PV), or indirectly using concentrated solar power (CSP).

Figure 2-1 Solar Panels to capture solar energy and produce electricity

A photovoltaic system converts light into electrical direct current (DC) by taking advantage of the photoelectric effect. Solar PV has turned into a multi-billion, fast-growing industry, continues to improve its cost-effectiveness, and has the most potential of any renewable technologies together with CSP. Concentrated solar power (CSP) systems use lenses or mirrors and tracking systems to focus a large area of sunlight into a small beam. Commercial concentrated solar power plants were first developed in the 1980s. CSP-Stirling has by far the highest efficiency among all solar energy technologies.

Figure 2-2 Concentrated Solar Power (CSP) - Solar Tower

In 2011, the International Energy Agency said that "the development of affordable, inexhaustible and clean solar energy technologies will have huge longer-term benefits. It will increase countries' energy security through reliance on an indigenous, inexhaustible and mostly import-independent resource, enhance sustainability, reduce pollution, lower the costs of mitigating climate change, and keep fossil fuel prices lower than otherwise. These advantages are global. Hence the additional costs of the incentives for early deployment should be considered learning investments; they must be wisely spent and need to be widely shared". In 2013 solar generated less than 1% of the world's total grid electricity.

2.2.2 Bio Energy

Biomass is biological material derived from living, or recently living organisms. It most often refers to plants or plant-derived materials which are specifically called lignocellulosic biomass. As an energy source, biomass can either be used directly via combustion to produce heat, or indirectly after converting it to various forms of biofuel. Conversion of biomass to biofuel can be achieved by different methods which are broadly classified into: thermal, chemical, and biochemical methods. Wood remains the largest biomass energy source today; examples include forest residues – such as dead trees, branches and tree stumps, yard clippings, wood chips and even municipal solid waste. In the second sense, biomass includes plant or animal matter that can be converted into fibers or other industrial chemicals, including biofuels. Industrial biomass can be grown from numerous types of plants, including miscanthus, switchgrass, hemp, corn, poplar, willow, sorghum, sugarcane, bamboo, and a variety of tree species, ranging from eucalyptus to oil palm (palm oil).

Plant energy is produced by crops specifically grown for use as fuel that offer high biomass output per hectare with low input energy. Some examples of these plants are wheat, which typically yield 7.5–8 tonnes of grain per hectare, and straw, which typically yield 3.5–5 tonnes per hectare in the UK. The grain can be used for liquid transportation fuels while the straw can be burned to produce heat or electricity. Plant biomass can also be degraded from cellulose to glucose through a series of chemical treatments, and the resulting sugar can then be used as a first generation biofuel.

Figure 2-3 Biomass Gasification base Power Plant

Biomass can be converted to other usable forms of energy like methane gas or transportation fuels like ethanol and biodiesel. Rotting garbage, and agricultural and human waste, all release methane gas – also called landfill gas or biogas. Crops, such as corn and sugarcane, can be fermented to produce the transportation fuel, ethanol. Biodiesel, another transportation fuel, can be produced from left-over food products like vegetable oils and animal fats. Also, biomass to liquids (BTLs) and cellulosic ethanol are still under research. There is a great deal of research involving algal fuel or algae-derived biomass due to the fact that it's a non-food resource and can be produced at rates 5 to 10 times those of other types of land-based agriculture, such as corn and soy. Once harvested, it can be fermented to produce biofuels such as ethanol, butanol, and methane, as well as biodiesel and hydrogen. The biomass used for electricity generation varies by region. Forest by-products, such as wood residues, are common in the United States. Agricultural waste is common in Mauritius (sugar cane residue) and Southeast Asia (rice husks). Animal husbandry residues, such as poultry litter, are common in the United Kingdom.

Biofuels include a wide range of fuels which are derived from biomass. The term covers solid, liquid, and gaseous fuels. Liquid biofuels include bio-alcohols, such as bio-ethanol, and oils, such as biodiesel. Gaseous biofuels include biogas, landfill gas and synthetic gas. Bio-ethanol is an alcohol made by fermenting the sugar components of plant materials and it is made mostly from sugar and starch crops. These include maize, sugarcane and, more recently, sweet sorghum. The latter crop is particularly suitable for growing in dry land conditions, and is being investigated by International Crops Research Institute for the Semi-Arid Tropics for its potential to provide fuel, along with food and animal feed, in arid parts of Asia and Africa.

With advanced technology being developed, cellulosic biomass, such as trees and grasses, are also used as feed stocks for ethanol production. Ethanol can be used as a fuel for vehicles in its pure form, but it is usually used as a gasoline additive to increase octane and improve vehicle emissions. Bio-ethanol is widely used in the United States and in Brazil. The energy costs for producing bio-ethanol are almost equal to, the energy yields from bio-ethanol. However, according to the European Environment Agency, biofuels do not address global warming concerns. Biodiesel is made from vegetable oils, animal fats or recycled greases. It can be used as a fuel for vehicles in its pure form, or more

commonly as a diesel additive to reduce levels of particulates, carbon monoxide, and hydrocarbons from diesel-powered vehicles. Biodiesel is produced from oils or fats using transesterification and is the most common biofuel in Europe. Biofuels provided 2.7% of the world's transport fuel in 2010.

Biomass, biogas and biofuels are burned to produce heat/power and in doing so harm the environment. Pollutants such as sulphurous oxides (SOx), nitrous oxides (NOx), and particulate matter (PM) are produced from the combustion of biomass; the World Health Organization estimates that 7 million premature deaths are caused each year by air pollution. Biomass combustion is a major contributor. The life cycle of the plants is sustainable, the lives of people less so.

2.2.3 Biogas

Biogas typically refers to a mixture of different gases produced by the breakdown of organic matter in the absence of oxygen. Biogas can be produced from raw materials such as agricultural waste, manure, municipal waste, plant material, sewage, green waste or food waste. It is a renewable energy source and in many cases exerts a very small carbon footprint. Biogas can be produced by anaerobic digestion with anaerobic bacteria, which digest material inside a closed system, or fermentation of biodegradable materials. Biogas is primarily methane (CH_4) and carbon dioxide (CO_2) and may have small amounts of hydrogen sulfide (H_2S), moisture and siloxanes. The gases methane, hydrogen, and carbon monoxide (CO) can be combusted or oxidized with oxygen. This energy release allows biogas to be used as a fuel; it can be used for any heating purpose, such as cooking. It can also be used in a gas engine to convert the energy in the gas into electricity and heat.

Figure 2-4 Biogas Plant

Biogas can be compressed, the same way natural gas is compressed to CNG, and used to power motor vehicles. In the UK, for example, biogas is estimated to have the potential to replace around 17% of vehicle fuel. It qualifies for renewable energy subsidies in some parts of the world. Biogas can be cleaned and upgraded to natural gas standards, when it becomes bio methane.

2.2.4 Wind Energy

Airflows can be used to run wind turbines. Modern utility-scale wind turbines range from around 600 kW to 5 MW of rated power, although turbines with rated output of 1.5–3 MW have become the most common for commercial use; the power available from the wind is a function of the cube of the wind speed, so as wind speed increases, power output increases up to the maximum output for the particular turbine. Areas where winds are stronger and more constant, such as offshore and high altitude sites are preferred locations for wind farms. Typically full load hours of wind turbines vary between 16 and 57 percent annually, but might be higher in particularly favorable offshore sites.

Globally, the long-term technical potential of wind energy is believed to be five times total current global energy production, or 40 times current electricity demand, assuming

all practical barriers needed were overcome. This would require wind turbines to be installed over large areas, particularly in areas of higher wind resources, such as offshore. As offshore wind speeds average ~90% greater than that of land, so offshore resources can contribute substantially more energy than land stationed turbines. In 2013 wind generated almost 3% of the world's total electricity.

Figure 2-5 Wind Power Plant

2.2.5 Hydro Energy

Since water is about 800 times denser than air, even a slow flowing stream of water, or moderate sea swell, can yield considerable amounts of energy. There are many forms of water energy:

Hydroelectric energy is a term usually reserved for large-scale hydroelectric dams. The largest of which is the Three Gorges Dam in China and a smaller example is the Akosombo Dam in Ghana.

Micro hydro systems are hydroelectric power installations that typically produce up to 100 kW of power. They are often used in water rich areas as a remote-area power supply (RAPS).

Run-of-the-river hydroelectricity systems derive kinetic energy from rivers without the creation of a large reservoir.

Figure 2-6 Hydro Power Plant

Hydropower is produced in 150 countries, with the Asia-Pacific region generating 32 percent of global hydropower in 2010. For counties having the largest percentage of electricity from renewables, the top 50 are primarily hydroelectric. China is the largest hydroelectricity producer, with 721 terawatt-hours of production in 2010, representing around 17 percent of domestic electricity use. There are now three hydroelectricity stations larger than 10 GW: the Three Gorges Dam in China, Itaipu Dam across the Brazil/Paraguay border, and Guri Dam in Venezuela. In 2013 hydropower generated almost 16% of the world's total electricity.

2.2.6 Geothermal Energy

Geothermal energy is from thermal energy generated and stored in the Earth. Thermal energy is the energy that determines the temperature of matter. Earth's geothermal energy originates from the original formation of the planet and from radioactive decay of minerals (in currently uncertain but possibly roughly equal proportions). The geothermal gradient, which is the difference in temperature between the core of the planet and its surface, drives a continuous conduction of thermal energy in the form of heat from the core to the surface. The adjective geothermal originates from the Greek roots geo, meaning earth, and thermos, meaning heat. The heat that is used for geothermal energy

can be from deep within the Earth, all the way down to Earth's core – 4,000 miles (6,400 km) down. At the core, temperatures may reach over 9,000 °F (5,000 °C). Heat conducts from the core to surrounding rock. Extremely high temperature and pressure cause some rock to melt, which is commonly known as magma. Magma convects upward since it is lighter than the solid rock. This magma then heats rock and water in the crust, sometimes up to 700 °F (371 °C).

From hot springs, geothermal energy has been used for bathing since Paleolithic times and for space heating since ancient Roman times, but it is now better known for electricity generation.

2.2.7 Other Energy Sources

2.2.7.1 Wave Energy

Wave power, which captures the energy of ocean surface waves, and tidal power, converting the energy of tides, is two forms of hydropower with future potential; however, they are not yet widely employed commercially. A demonstration project operated by the Ocean Renewable Power Company on the coast of Maine, and connected to the grid, harnesses tidal power from the Bay of Fundy, location of world's highest tidal flow. Ocean thermal energy conversion, which uses the temperature difference between cooler deep and warmer surface waters, has currently no economic feasibility.

Figure 2-7 Power from Wave Energy

2.2.7.2 Tidal Energy

Tidal power, also called tidal energy, is a form of hydropower that converts the energy obtained from tides into useful forms of power, mainly electricity. Although not yet widely used, tidal power has potential for future electricity generation. Tides are more predictable than wind energy and solar power. Among sources of renewable energy, tidal power has traditionally suffered from relatively high cost and limited availability of sites with sufficiently high tidal ranges or flow velocities, thus constricting its total availability. However, many recent developments and improvements, both in design (e.g. dynamic tidal power, tidal lagoons) and turbine technology (e.g. new axial turbines, cross flow turbines), indicate that the total availability of tidal power may be much higher than previously assumed, and that economic and environmental costs may be brought down to competitive levels.

2.2.7.3 Heat pump

A heat pump is a device that provides heat energy from a source of heat to a destination called a "heat sink". Heat pumps are designed to move thermal energy opposite to the direction of spontaneous heat flow by absorbing heat from a cold space and releasing it to a warmer one. A heat pump uses some amount of external power to accomplish the work of transferring energy from the heat source to the heat sink.

2.2.7.4 Grid Energy Storage

Grid energy storage (also called large-scale energy storage) is a collection of methods used to store electrical energy on a large scale within an electrical power grid. Electrical energy is stored during times when production (especially from intermittent power plants such as renewable electricity sources such as wind power, tidal power, and solar power) exceeds consumption, and returned to the grid when production falls below consumption.

2.3 Solar Energy Technology

Solar energy systems are two types: Solar photovoltaic system (Uses photon energy from sun to generate electricity) and Concentrated solar power system (uses thermal energy from sun).

2.3.1 Solar Photovoltaic System

Photovoltaic (PV) materials and devices convert sunlight into electrical energy, and PV cells are commonly known as solar cells. Photovoltaics can literally be translated as light-electricity.

First used in about 1890, "photovoltaic" has two parts: photo, derived from the Greek word for light, and volt, relating to electricity pioneer Alessandro Volta. And this is what photovoltaic materials and devices do—they convert light energy into electrical energy, as French physicist Edmond Becquerel discovered as early as 1839.

Becquerel discovered the process of using sunlight to produce an electric current in a solid material. But it took more than another century to truly understand this process. Scientists eventually learned that the photoelectric or photovoltaic effect caused certain materials to convert light energy into electrical energy at the atomic level.

PV systems are already an important part of our daily lives. Simple PV systems provide power for small consumer items such as calculators and wristwatches. More complicated systems provide power for communications satellites, water pumps, and the lights, appliances, and machines in some homes and workplaces. Many road and traffic signs also are now powered by PV. In many cases, PV power is the least expensive form of electricity for these tasks.

Photovoltaic system consists of solar module, which is comprises with many solar cells. To obtain electricity solar cell plays a vital role in the system. Hence various research are going on to develop optimize level solar cell to get best possible electricity. As in concern to that, this research is conducted to get viable cell performance using unorthodox solar cell technology.

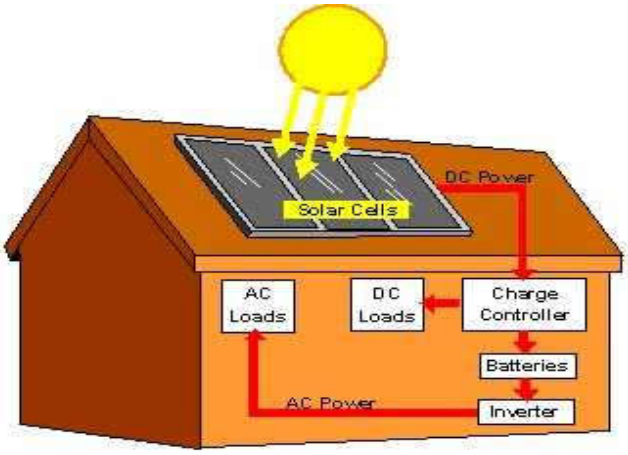

Figure 2-8 Solar Photovoltaic System for Household Electricity Production

3 Chapter 3

3.1 Solar Cell

3.1.1 Solar Cell

A solar cell or photovoltaic cell is a device which generates electricity directly from visible light by means of the photovoltaic effect, which is a physical and chemical phenomenon. It is a form of photoelectric cell, defined as a device whose electrical characteristics, such as current, voltage, or resistance, vary when exposed to light. Solar cells are the building blocks of photovoltaic modules, otherwise known as solar panels.

3.2 Different Generations of Solar Cells

Solar cells are usually divided into three main categories called generations. The first generation contains solar cells that are relatively expensive to produce, and have a low efficiency. The second generation contains types of solar cells that have an even lower efficiency, but are much cheaper to produce, such that the cost per watt is lower than in first generation cells. The term third generation is used about cells that are very efficient. Most technologies in this generation are not yet commercial, but there is a lot of research going on in this area. The goal is to make third generation solar cells cheap to produce.

3.2.1 First Generation Solar Cells

The first generation includes cells consisting of Silicon or Germanium that are doped with Phosphorus and Boron in a pn-junction. This generation is dominating the commercial market. Silicon cells have a quite high efficiency, but very pure silicon is needed, and due to the energy-requiring process, the price is high compared to the power output.

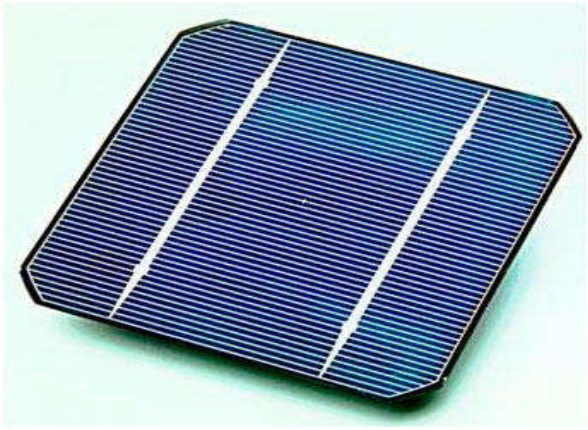

Figure 3-1Multicrystalline silicon solar cell

3.2.2 Second Generation Solar Cells

The second generation solar cells are based on amorphous silicon, CIGS and CdTe, where the typical performance is 10 - 15%. Since the second generation solar cells avoid use of silicon wafers and have a lower material consumption it has been possible to reduce production costs of these types of solar cells compared to the first generation. The second generation solar cells can also be produced so they are flexible to some degree. However, as the production of second generation solar cells still include vacuum processes and high temperature treatments, there is still a large energy consumption associated with the production of these solar cells. Further, the second generation solar cells are based on scarce elements and this is a limiting factor in the price.

3.2.2.1 Amorphous Silicon Solar Cells

In Amorphous Silicon Cells, hydrogen is introduced to the silicon to make it possible to dope the silicon with boron and phosphorus. The cells are built up in this sequence from bottom to top: metal base contact, n-layer, intrinsic layer, p-layer, transparent contact, glass substrate. These cells experience a drop in efficiency when they are exposed to sunlight, and this effect is created in the intrinsic layer. The effect can be reduced by, instead of one layer, using several thinner layers.

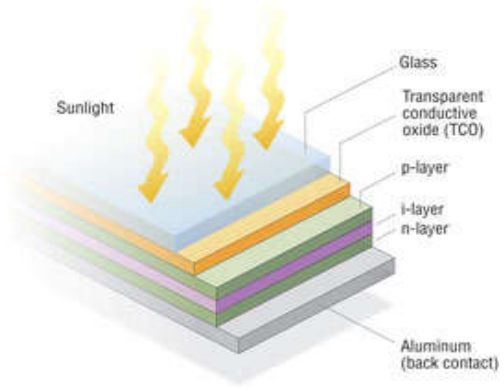

Figure 3-2 Amorphous Silicon Solar Cell

3.2.2.2 Polycrystalline Silicon on Low Cost Substrate

These cells use antireflection layers to capture light waves with wavelengths several times greater than the thickness of the cell itself. This can be done by using a material with a textured surface both in front and back of the cell, rather than a flat surface. This causes the light to change directions and be reflected, and thus travels a greater distance within the cell then the cell thickness.

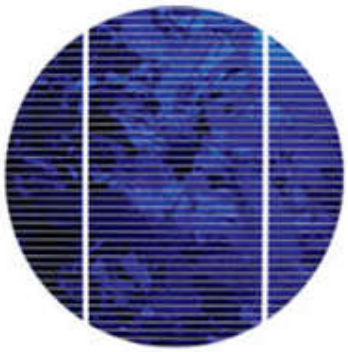

Figure 3-3 Polycrystalline Silicon Solar Cell

3.2.2.3 Copper Indium DiSelenide (CIS) Cells

Copper Indium Diselenide consists of $CuInSe_2$. This material is one of the best light absorber known, and about 99% of the light is absorbed before reaching 1 μm into the material. There have been made homojunctions of CIS, but a heterojunction with cadmium sulfide (CdS) has been found to be more stable and efficient.

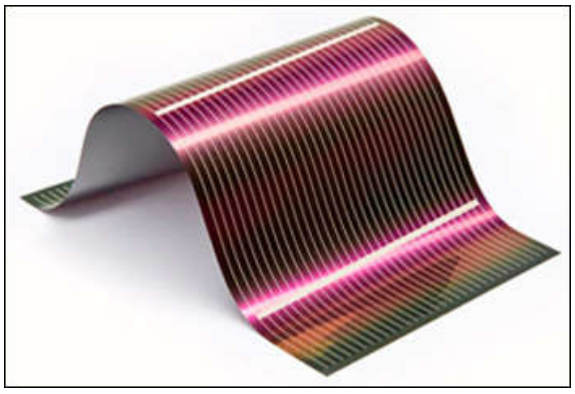

Figure 3-4 Flexible Copper Indium Gallium diSelenide solar cells

3.2.2.4 Cadmium Telluride Solar Cells

These cells are made from a heterojunction with cadmium sulfide, just like the copper indium diselenide. Cadmium telluride cells also have an ideal bandgap (1.44eV).

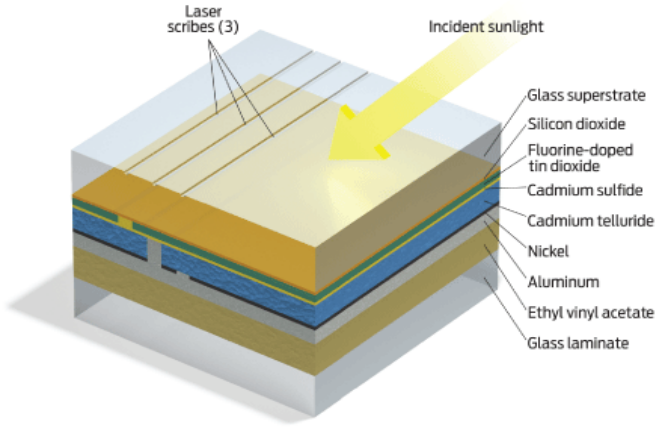

Figure 3-5 Schematic of Cadmium Telluride Solar Cells

3.2.3 Third Generation Solar Cells

3.2.3.1 Quantum Dot (QD) Solar Cells

There are several technologies in this generation. One of them is Quantum Dot (QD) Solar Cells. These are built up of a semiconductor (silicon) coated with a very thin layer of quantum dots. Quantum dots is just a fancy name of crystals in the size range typically a few nanometers in diameter. These crystals are mixed into a solution and placed on a piece of silicon which is rotated really fast. The crystals are then spread out due to the centrifugal force. The reason these quantum dots are given so much attention is that normally one photon will excite one electron creating one electron-hole pair. The energy loss is the original energy of the photon minus the energy needed to excite the electron(also called the band gap) However, when a photon hits a quantum dot made of

the same material, there may be several electron-hole pairs created, typically 2-3, but 7 has been observed.

Another way to increase the efficiency is to use several layers solar cells with different band gaps in a stack. Each layer will utilize light with different wavelengths, and in this way we can get cells with a higher efficiency.

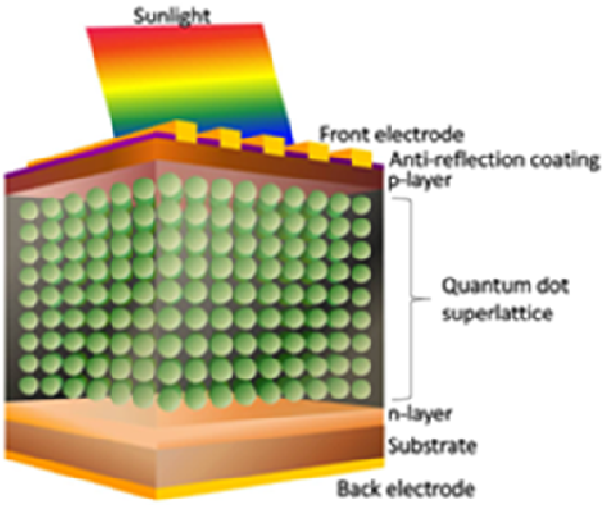

Figure 3-6 Schematic of Quantum Dot (QD) Solar Cells

3.2.3.2 Multijunction Solar Cells

Another way to increase the efficiency is to use several layers solar cells with different band gaps in a stack. Each layer will utilize light with different wavelengths, and in this way we can get cells with a higher efficiency.

3.2.3.3 Dye-Sensitized Solar Cells

M. Grätzel of the Swiss Polytechnic of Lausanne discovered a thin-film titanium dioxide system that is sensitive to ultraviolet radiation can be made to respond to ordinary light. A layer of light-responsive dye overlays the semiconductor and the charge is transferred back to the dye from an electrolyte. The cells have reasonable efficiencies (~ 10%) in hazy light conditions, and the cost is projected to be very low, since the materials can be worked on at low temperatures in contrast to most other semiconductor solar cell arrays.

A new idea to harvest solar energy uses dyes on a metal substrate, quite different from what occurs in normal silicon solar cells. The device developed by McFarland and Tang has multiple layers on ultrathin metal films that constitute a Schottky diode (a diode that works by quantum tunneling).

Electrons excited to a higher state by incident light can jump the Schottky barrier and so provide a current. The efficiency is higher than expected. As McFarland and Tang say, "This alternative approach to photovoltaic energy conversion might provide the basis for durable low-cost solar cells using a variety of materials."

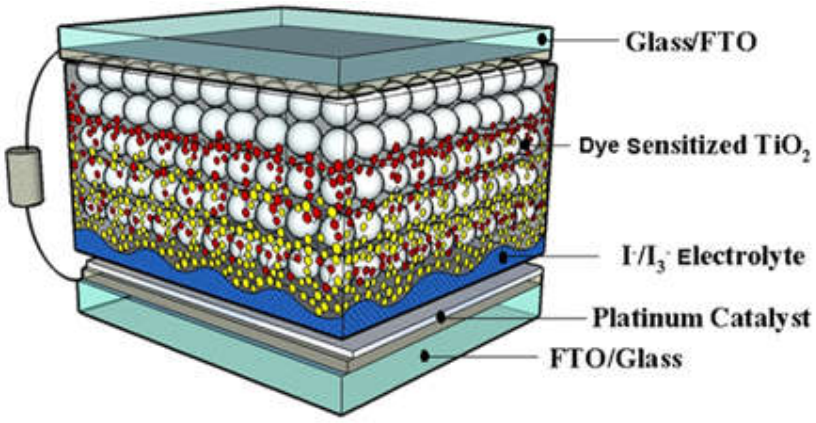

Figure 3-7 Schematic of Dye Sensitized Solar Cell

3.3 Solar Cell Terminologies

A current source in parallel with a forward biased diode expresses the equivalent circuit of an ideal solar cell. Series and parallel resistances are added to account for various loss mechanisms.

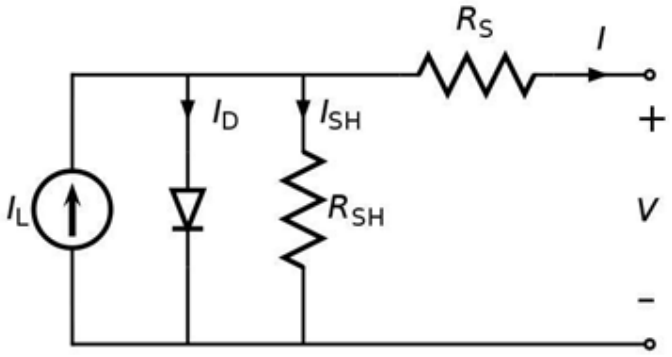

Figure 3-8 Solar cell equivalent circuit

3.3.1 Short-Circuit Current

It is the current obtained from the cell when short circuited or in other words when the load resistance is zero. Solar cell current is normally represented as current density, Jsc:

$$J_{sc} = {}^{Isc}/_{A} \text{ mA/cm}^2 \qquad 1.1$$

Where, A is the effective area of the solar cell. It is a function of the solar illumination, optical properties and charge transfer probability of the cell.

3.3.2 Open-Circuit Voltage

Open-circuit voltage is the maximum voltage available from a solar cell and is obtained when a load with infinite resistance is attached to its terminals. It is a function of the semiconductor bandgap and charge recombination in the cell. For DSC the Voc is given by:

$$V_{oc} = E_{CB}/q + kT/q \ln (n/N_{CB}) E_{redox}/q \text{ (Volts)} \quad 1.2$$

Where, n is the number of electron in TiO_2 conduction band and NCB is the effective density of states75. The first two terms defines the quasi-fermi level of TiO_2 and Eredox is the Nernst potential of the redox mediator.

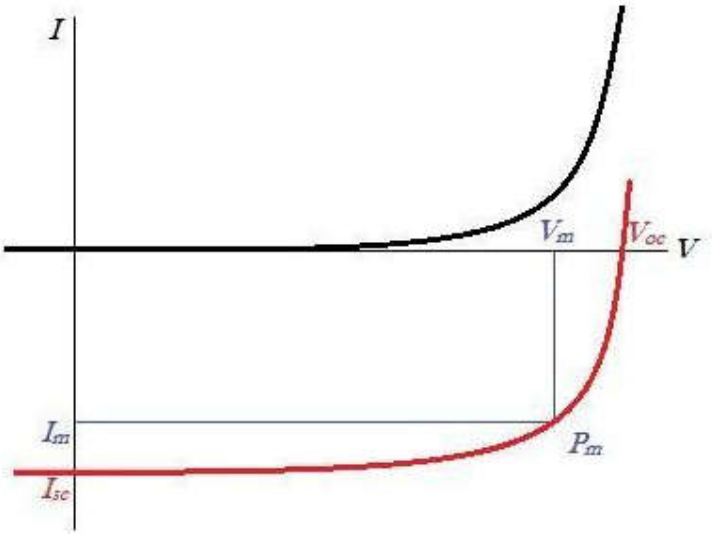

Light I-V response (red line) and dark I-V response (Black line)

Figure 3-9 Typical current-voltage relationship of a solar cell

3.3.3 Series Resistance

Series resistance, RS in a solar cell is the result of contact resistance and charge transfer resistance in the semiconductor material. Series resistance reduces the fill factor affecting the maximum power output, while excessively high value of RS can also reduce the

short-circuit current. The open-circuit voltage is not affected since, at V_{OC} the total current flow through cell itself and hence through the series resistance is zero. An approximation of the series resistance can be determined from the slope of the I-V curve at the open-circuit voltage point.

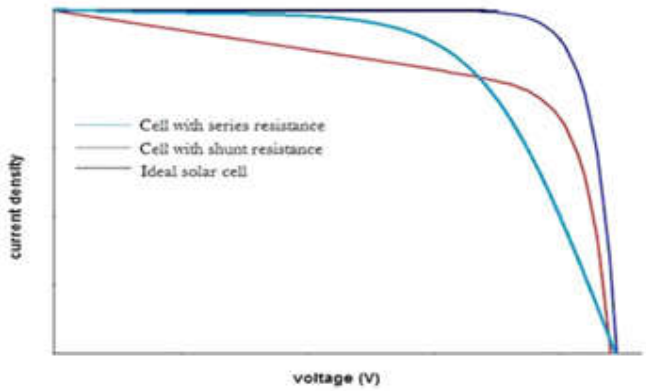

Figure 3-10 Current-voltage response of a solar cell with series and shunt resistance

3.3.4 Shunt Resistance

Low shunt resistance provides an alternate current path for the photo-generated current causing significant power loss. The effect of low shunt resistance is reduced fill factor and lower open-circuit voltage affecting the maximum power output. The short-circuit voltage is not affected unless for a very low value, since at J_{SC} the total current flows through the outer path and hence through the shunt resistance is low. An approximation of the shunt resistance can be calculated from the slope of the IV curve at the short circuit current point.

3.3.5 Fill Factor

The fill factor (FF) is a measure of the maximum power output from a solar cell. It represents the squareness of the I-V curve and is defined as the ratio of the maximum power to the product of V_{OC} and I_{SC} for the solar cell:

FF = VmIm/ VocIsc 1.3

Where, Vm and Im are the voltage and current at maximum power point. Fill factor, being a ratio of the same physical parameters, has no unit. Fill factor is a function of the series and shunt resistance of the solar cell. For DSC, it reflects the extent of electrical and electrochemical losses during cell operation. To obtain higher fill factor improvement of the shunt resistance and decrement of the series resistance, with reduction of the overvoltage for diffusion and charge transfer is required.

3.3.6 Efficiency

The efficiency of a solar cell is defined as the ratio of maximum electrical energy output to the energy input from the sun. Thus the mathematical definition of Efficiency:

$\eta = (Voc \times Isc \times FF) / Pin$ 1.4

Where, Pin is the power input from the sunlight. Efficiency is generally expressed in percentage.

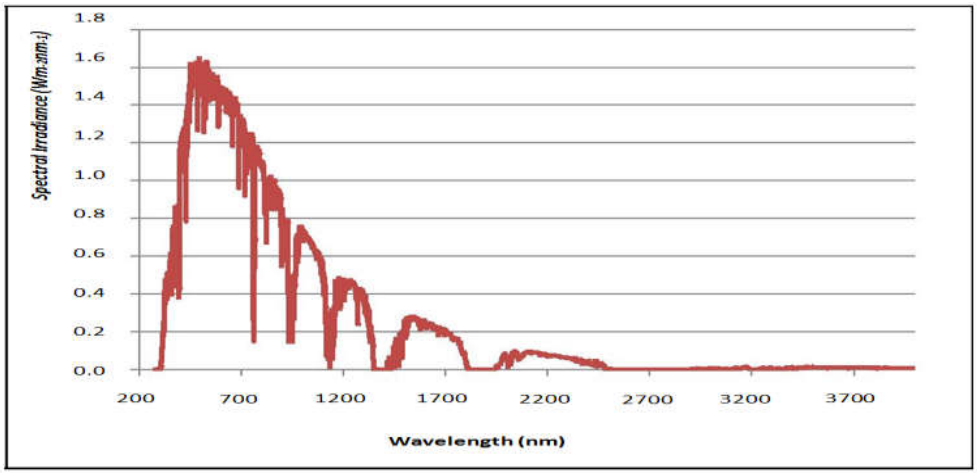

Figure 3-11 'AM1.5 Global' spectra for solar cell measurement

Besides the solar cell performance itself, it depends on the incident light spectrum and intensity as well as operating temperature. The internationally recognized standard condition for the efficiency measurement of solar cells is under 'AM1.5 Global' 76 solar irradiation and at a temperature of 25°C. (Fig. 1.6)

3.3.7 Quantum Efficiency

Quantum efficiency (QE) or 'External Quantum Efficiency (EQE)', sometimes also referred to as Incident Photon to Charge Carrier Efficiency (IPCE) is a measure of how efficient a solar cell is in producing photo-generated charge at a given frequency. It is defined as the ratio of the number of incident photons to the number of charge carriers generated and is a function of the excitation wavelength:

$$IPCE\ (\lambda) = 1240 \times Isc/\lambda \times \varphi \qquad 1.5$$

Where, ISC is the short circuit current (mA/cm^2), λ is the wavelength (nm) and Φ is the incident radiative light flux (W/m^2).

For DSC, the term is defined as:

$$IPCE\ (\lambda) = LHE\ (\lambda) \times \varphi\ (inj) \times \eta\ (coll) \qquad 1.6$$

Where, LHE (λ) is the light-harvesting efficiency for photons at wavelength λ, Φ (inj) is the electron injection quantum yield for the excited sensitizer to the semiconductor oxide conduction band and η (coll) is the fraction of injected charges that is able to reach the back contact77.

4 Chapter 4

4.1 TiO_2 Dye-Sensitized Solar Cell Using Dye

4.1.1 TiO_2 Dye-Sensitized Solar Cell

Dye-sensitized cells, which are less efficient, but are far less expensive to manufacture. The dye absorbs light and transfers the excited electrons to the titanium dioxide. The titanium dioxide semiconductor material separates the charge. The redox couple completes the circuit. In this thesis research, we have usedRed Amaranth (Scientific name: Amaranthasgangetica) juice to construct a dye-sensitized solar cell and measure the electricity the cell produces.

Highly porous nanoparticle films were investigated as alternative working electrode morphology for the synthesis of dye sensitized solar cells (DSSCs). These films were rapidly assembled by flame synthesis and direct aerosol deposition of TiO2 nanoparticles with high specific surface area. Structural–functional analysis of their properties revealed that the film porosity is a key parameter greatly determining the resulting energy conversion efficiency (η). In fact, aerosol deposition at low substrate temperatures (~100 °C) led to very high porosity (ε = 98%) and weak film cohesion. These films were easily resuspended upon immersion in the dye and/or electrolyte solutions resulting in very poor performances (η = 0.08%). In contrast, allowing for partial nanoparticle sintering by deposition at moderate temperatures (~400 °C) decreased the film porosity from 98 to 95% leading to higher mechanical stability and partially preserving the large surface required for dye adsorption. As a result, these films had drastically higher current density (12.2 mA cm−2) and overall performances (η = 5%) representing an 8 times improvement with respect to the best reported for similar highly porous morphologies. Remarkably, their conversion efficiency decreased only slightly with increasing film thickness reaching 4.6% at 128 μm. This unique attribute suggests that high film porosity may inhibit recombination losses enabling utilization of thick films with enhanced light absorption properties.

4.1.2 Advantages of DSSC over Crystalline Solar Cell

- Technology is relatively simple and inexpensive for DSSC solar cell.
- Low-light performance: DSSC works in a wide array of lighting conditions that makes it suitable for a diverse range of shaded and diffuse light locations, without suffering from angular dependence of sunlight or light.
- Optimised performance: DSSC materials and dyes can be tuned for optimisation in a variety of lighting conditions making it suitable for indoor applications and outdoor applications.
- Higher temperature performance: Efficiency of DSSC does not degrade with increased temperature, meaning you can continue to efficiently harvest energy in direct sunlight.
- Low energy manufacturing process: DSSC is manufactured using a low-energy consumption, high-efficiency, roll-to-roll manufacturing technique.
- Ecologically friendly solar: DSSC uses inexpensive and eco-friendly nano-materials without concern about shortage of resources.
- Variety of substrates: DSSC is produced on a thin film, flexible, robust, plastic substrate. DSSC can also be applied to metal and glass substrates.
- Versatile product integration: DSSC indoor modules are highly flexible, durable and lightweight. As a result they are very versatile and can be incorporated into a wide variety of products.

4.1.3 TiO_2 Thin Film Photo Electrode

Titanium dioxide (TiO_2) is a stable, nontoxic oxide, is environmentally friendly, and has a high refractive index. TiO_2 represents one of the most important compounds of titanium and oxygen, and is an extremely versatile material, suitable for a variety of technological applications [1-3]. TiO_2 exists in three distinct crystalline polymorphs: rutile, anatase, and brookite, shown in Figure 4.1. Mainly, however, TiO_2 exists in the anatase and rutile phases. These two structures can be described in terms of chains of TiO_6octahedra, where each Ti^{4+} ion is surrounded by an octahedron of six O^{2-} ions. The

anatase and rutile crystal structures differ in the distortion of each octahedron and by the assembly pattern of the octahedra chains(Figures1.1(a) and (b))[7].In rutile, each octahedron shares corners with eight neighbors and shares edges with two other neighbors, forming a linear chain. In anatase, each octahedron shares corners with four neighbors and shares edges with four other neighbors, forming a zigzag chain with a screw axis. Thus, anatase is less dense than rutile. In addition, anatase has a large metal–metal distance of 5.35 Å. As a consequence, the Ti dxyorbitals at the bottom of the conduction band are quite isolated, while the $t_2$gorbitals at the bottom of the conduction band in rutile provide the metal–metal interaction with a smaller distance of 2.96 Å [7].Rutile is the most common natural form of titania [8] and is the most thermodynamically stable form. TiO_2has a wide band gap (3.2 eV for anatase and 3.0 eV for rutile) and an optical penetration depth of δp= 250 nm at λ = 308 nm of incident light [9]($\delta p$is defined as the depth at which the intensity of the incident light decays to 1/e of the original value). Anatase TiO_2has several advantages over the rutile phase in terms of the charge dynamics. First, it has better charge carrier mobility and a longer charge carrier lifetime[10].Second, it exhibits a thicker depletion layer and stronger band bending [11-12]. As a result, surface hole trapping dominates the spatial chargeseparation in anatase, owing to the strong upward band bending (with a longer minority (hole) diffusion length, 70 nm in anatase [13] vs. 10 nm in rutile [14]). In rutile, bulk recombination of electrons and holes prevails since only the holes very close to the surface can migrate to the surface [10, 15]. Anatase TiO_2 exhibits a charge recombination rate around ten times lowers than that of rutile [16]. Third, anatase has a key role in the injection and transport of electrons in photovoltaic devices, owing to the moderate band gap [17].

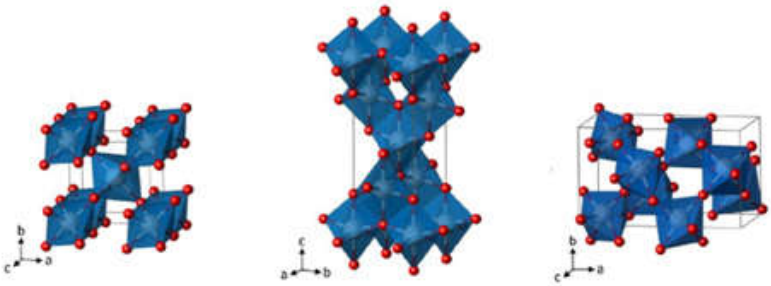

(a) Rutile (b) Anatase (c) Brookite

(d)	Crystal system	Density [g/cm^3]	Optical band-gap [eV]	Refractive index
Rutile	tetragonal	4.13 - 4.26	3.0	2.72
Anatase	tetragonal	3.79 - 3.84	3.19	2.52
Brookite	orthorhombic	3.99 - 4.11	3.11	2.63

Figure 4-1 Crystal structures of TiO6 polyhedra for the (a) rutile, (b) anatase, and (c) brookite phases of TiO_2Ti is depicted in white, O in red. Lattice parameters: a = b = 4.5937 Å, c = 2.9581 Å for rutile; a = b = 3.7842 Å, c = 9.5146 Å for anatase; and a = 9.16 Å, b = 5.43 Å, and c = 5.13 Å for brookite [14]. (d) The physical properties of each crystal structure [4, 15]

Titanium dioxide (TiO_2) can be used in the creation of photoelectrodes for the production of Dye Sensitized, Perovskite and other solid state solar cells. $TiO_2$is a wide band gap inorganic semiconductor substance that is thermally stable, non-flammable, insoluble, and not classified as hazardous by Globally Harmonized System of Classification and Labeling of Chemicals (GHS). Nanostructured titanium oxides are used in lithium ion batteries, electrochromic devices, solid oxide fuel cells and photovoltaics. In 2013 the annual production of $TiO_2$was more than 5 million tonnes, with an addressable market of over $10 billion.1 Commodity grade TiO_2 nanoparticles are very cheap as they are made from inexpensive minerals using chloride or sulfate process. They are often contaminated with many metallic impurities, which are known traps for electronic applications. They also exist in aggregate forms with 20 to 30% rutile impurities that are hard to disperse for transparent coating applications. Although high anatase content can be achieved using sulfate process, it is hard to remove sulfate groups during sintering of sulfate process derived TiO_2. The sulfate groups move to surface of the nanoparticles during sintering and interfere with dyeing process resulting in low performing DSSC.

Fujishima and Honda[18] first discovered the phenomenon of photocatalytic splitting of water over a TiO_2electrode under ultraviolet light in 1972. The effective utilization of clean, safe and abundant solar energy through the TiO_2photocatalysis provides promising solutions to the energy crisis and serious environmental challenges. TiO_2has been widely used commercially inpigments, [19] sunscreens, [20], [21] paints, [22]toothpaste,[23]etc. Mesoporous materials [24],[25] have a wide range of applications, including their important role in photoelectrochemical cells, photocatalystsandsensors, water splitting for the creation of hydrogen, gas sensing, coated fabrics and textiles, catalyst systems, ceramics, floor coverings, roofing materials, corrosion protective coating, optical coating, biocompatible coatings in orthopedic implants, varistors, and incosmetics a paper industry.

Dye sensitized solar cells (DSSCs) as alternatives to traditional silicon-based solar cell devices have attracted widespread attention due to their clean and pollution free nature, easy fabrication and powerful harvesting efficiency.[26] One of the key elements in DSSC is the mesoporous TiO_2photoanode, which transfers the charge carriers from the sensitizer (dye) to the fluorine-doped tin oxide (FTO) electrode and concurrently allows the electrolytes (redox couples) to diffuse to the anchored dyes. Typically, nanoparticles are used for the fabrication of the mesoporous TiO_2layers on the FTO to obtain high surface areas and generate nanopored structures.[27],[28] In general, upon decreasing the size of TiO_2nanoparticles, the surface area of the fabricated nanoporousTiO2 film is increased, and thus more dye molecules can be adsorbed. However, the average pore size is decreased simultaneously, and more defect sites and grain boundaries can be generated in the fabricated TiO_2film. These defects will affect efficiency of DSSC. Kim et al29reported that nanoporous spherical structures will provide both high adsorption of dye molecules and efficient electrolyte diffusion. In addition, the spherical TiO_2 structures offer a considerable scattering effect in the long-wavelength region. Generally, TiO_2 contains three different phases (anatase,rutile and brookite). Among them anatase and rutile phasesare having severalapplications. The optical band gap of TiO_2nanostructures with anatase phase is 3.2 eV, whereas for the rutile it is 3.0 eV.30The anatase conduction band is 0.2 eV more negative than that of rutile if the same redox material is employed. This will cause more open-circuit voltage in DSSC than rutile phase.

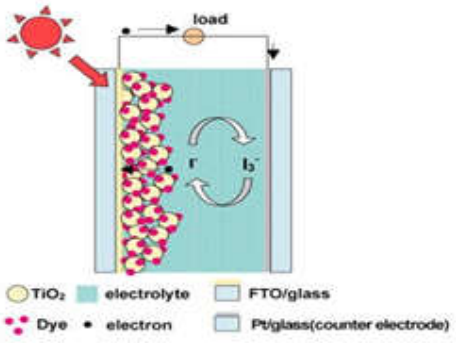

Figure 4-2 TiO_2 DSSC Photo Electrode

4.1.4 Natural Pigments Used in DSSCs

Based on the results with Ru-complexes also a variety of metal–organic dyes such as Zn porphyrin derivatives have been tested [34]. Prerequisites for photosensitizers to function in DSSCs are the absorption in the visible or near-infrared regions of the solar spectrum and the binding to the semiconductor TiO_2[35]. The functional group necessary to interact with the TiO_2 surface is a carboxylic or other peripheral acidic anchoring group [6] and [35]. The TiO_2 binding moiety of large π-aromatic molecules is very often a carboxylic group [37]. There are several possible chemical functional groups that are able to bind the dye to the TiO_2. The best anchoring groups for metal oxides are phosphonic acids followed by carboxylic acids and their derivatives, such as acid chlorides, amides, esters or carboxylate salts [36]. The carboxylic group is the most frequently used anchoring group. In order to form bonds, the dye's binding groups react with surface hydroxyl groups of the metal oxide. In the case of phosphonic acids or carboxylic acids, a reversible binding with high equilibrium binding constants is established between the photosensitizer and TiO_2. In basic conditions (usually pH $\geqslant$ 9) the dyes are easily desorbed again. There are several binding modes between the TiO2 and a dye molecule with at least one carboxylic group (COOH)[36], [38] and [39]. Which mode of chemisorption between $TiO_2$and COOH is prevalent depends on the dye's structure, its anchoring groups, the pH, and the metal oxide's preparation [36]. The interaction of

TiO2 with cyanin, an anthocyanidine, is via the hydroxyl-ketone tautomer of cyanin [35]. The main issues which have to be taken into account are an appropriate anchoring of the molecules while allowing a fast and energetically optimized charge transfer. The π electrons of the carboxylic group should be in resonance with the π electrons of the polyene backbone in order to be able to shift the electrons through the anchoring group into the conduction band of the semiconductor. The color of dyes also depends on such delocalized π electrons.Over 80 metal-free organic dyes that can be prepared by cheaper methods have been described [31]. The highest η was 9.5% with a novel indoline dye [40]. A special method for the modification of the TiO_2 layer with the metal-free organic dye D102 has recently been reported to result in a significant increase of η [41]. Natural dyes as photosensitizers for DSSCs are very attractive because they are of low cost, abundant in supply, and sustainable. An early proof that carotenoids can function as photosensitizers in DSSCs was with 8′-apo-β-caroten-8′-oic acid bound to TiO_2. A photocurrent stable for 1 h under continuous radiation was measured and an ordered monolayer structure of the TiO_2-bound carotenoid has been suggested [42]. Since then, carotenoids have already been successfully used in DSSCs [43], [44] and [45]. The highest η with single carotenoids was 2.6% [46]. The optimal length of carotenoids consists of seven conjugated π bounds [47]. By using carotenoids in combination with chlorophyll derivatives η can be increased to up to 4.2% [48]. This increase is probably due to similarities to photosynthesis. Several extracts have been discovered as efficient photosensitizers. The effect of a black rice extract has been attributed to an anthocyanin with an o-hydroxychinon moiety [49]. A different study showed that amongst 20 plant extracts a mangosteen pericarp extract showed the highest efficiency η of 1.17%. The active component has been described as rutin [50]. An overall comparison identified an extract of Rhoeospathacea with an efficiency η of 1.49% as attractive source amongst others [51]. The glycosides of anthocyanidins, the anthocyanins, seem to be more efficient than the anthocyanidins. An explanation could be the better solubility in H_2O. Nevertheless, the interaction of cyanidin with TiO_2 particles for the use in DSSCs was suggested already in 2007 [52]. The natural dyes used so far in DSSCs are summarized in Table 4.1. Data are often obtained under different conditions and device setups by different authors and therefore, they are in some cases difficult to compare directly. The photosensitizers belong to different chemical classes, which contain mainly carotenoids,

betalains, flavonoids, or chlorophylls. A high η of 2.06% was obtained with an extract of Sicilian prickly pear [43]. Promising natural carotenoids are crocetin or bixin.

Plant source	Structure or structural class	Photo active area (cm2)	Jsc(mA /cm2)	Voc(mV)	η/FF	Remark	Refere nce
Black rice	Anthocyanin	1	1.142	551	na/0. 52	Fractiona ted extract	[49]
ErythrinaVari egata	Carotenoid, Chlorophyll	1	0.776	484	na/0. 55	Fractiona ted extract	[49]
Rosa xanthina	Anthocyanin	1	0.637	492	na/0. 52	Fractiona ted extract	[49]
Kelp	Chlorophyll	1	0.433	441	na/0. 62	Fractiona ted extract	[49]
Capsicum	Carotenoid	1	0.225	412	na/0. 63	Fractiona ted extract	[49]
Begonia		0.2	0.63	537	0.24/ 0.72	Extract	[51]
Rhododendro n		0.2	1.61	585	0.57/ 0.61	Extract	[51]
Perilla		0.2	1.36	522	0.5/0	Extract	[51]

Plant source	Structure or structural class	Photo active area (cm2)	Jsc(mA /cm2)	Voc(mV)	η/FF	Remark	Refere nce
					.70		
Mangosteen pericarp		0.2	2.69	686	1.17/ 0.63	Extract	[51]
Mangosteen pericarp	α-Mangostin/β-mangostin	0.2	2.55	621	0.92/ 0.58	Fractiona ted extract	[51]
Mangosteen pericarp	Rutin	0.2	2.92	611	1.12/ 0.63	Fractiona ted extract	[51]
Hibiscus sabdariffa L.	Cyanidin-3-glycosides/del phinidin-3-glycoside	–	1.63	404	0.37/ 0.57	Aqueous extract	[53]
Beta vulgaris rubra	Betalains	0.5	9.5	425	1.7/0 .37	Aqueous extract	[54]
RhoeospathaceaStearn	–	–	10.9	496	1.5/0 .27	Ethanol extracts, aqueous electrolyt e	[55]
Bixaorellana L.	Bixin	0.5	1.1	570	0.37/ 0.59	Fractiona ted extract	[56]

Plant source	Structure or structural class	Photo active area (cm2)	Jsc(mA /cm2)	Voc(mV)	η/FF	Remark	Refere nce
Spinach	Modified chlorophyll/n eoxanthin	–	11.8	550	3.9/0 .60	Isolated compoun ds	[37]
Spinach	Modified chlorophyll/vi olaxanthin	–	11.4	540	3.7/0 .61	Isolated compoun ds	[48]
Spinach	Modified chlorophyll/lu tein	–	12.5	540	4.0/0 .59	Isolated compoun ds	[48] an d [48]
n.a.	Modified chlorophyll/β- carotene	–	13.7	530	4.2/0 .58	Isolated compoun ds	[48]
Chaste tree fruit	–	–	1.06x	390	na/0. 48	Extract	[57]
Mulberry	–	–	0.86x	422	na/0. 43	Extract	[57]
Cabbage-palm fruit	–	–	0.37x	442	na/0. 61	Extract	[57]
Calafate fruit	Delphinidin	–	0.96	520	na/0. 56	Aqueous extract	[58]
Jaboticaba skin	Peonidin	–	2.6	660	na/0. 62	Ethanolic extract	[58]

Plant source	Structure or structural class	Photo active area (cm2)	Jsc(mA /cm2)	Voc(mV)	η/FF	Remark	Refere nce
Gardenia fruit	Crocetin/	1.0	2.84	430	0.56/ 0.46	Isolated compoun ds	[59]
	crocin		0.45	580	0.16/ 0.60		
Red Sicilian orange ‘‘Moro’’	Cyanin	0.5– 1.0	3.84	340	0.66/ 0.50	Fruit juice	[60]
Eggplant skin	Nasunin	0.5– 1.0	3.40	350	0.48/ 0.40	Ethanolic extract	[60]
Prickly pear	Betaxanthin	1.0	8.8	389	2.06/ 0.60	Acidified juice	[61]
TradescantiaZ ebrina	Antocyanin	–	0.63	350	0.23/ 0.55	Ethanolic extract	[62]
Kapok	Antocyanin/c arotenoid	–	0.87	360	0.3/0 .49	Ethanolic extract	[62]
Pitaya	Not reported	–	0.5	330	0.17/ 0.52	Ethanolic extract	[62]
Canariumodo ntophyllum	Antocyanin	–	2.45	385	0.59/ 0.62	Ethanolic extract	[63]
Ixora sp.	Antocyanin	–	6.26	351	0.96/	Ethanolic	[63]

Plant source	Structure or structural class	Photo active area (cm2)	Jsc(mA /cm2)	Voc(mV)	η/FF	Remark	Refere nce
					0.44	extract	
C. odontophyllu m + Ixora sp.	Antocyanin	–	6.26	384	1.13/ 0.47	Mixed ethanolic extract	[63]
C. odontophyllu m + Ixora sp.	Antocyanin	–	9.80	343	1.55/ 0.46	Ethanolic extracts in consecuti ve layers	[63]
Rhododendro n sp.	Antocyanin	0.27	0.85	544	0.33/ 0.72	Ethanolic extract	[64]

Table 1 Natural dyes used in DSSCs

4.1.5 Dye-Sensitized Solar Cells

4.2 Solar Spectrum

The radiation of the sun can be well approximated by a black body at a temperature of 5800K emitting according to Planck's distribution [78].The power density of the Sun outside the Earth's atmosphere is given by the solar constant 1353 ± 21 Wm^{-2}, dropping to approximately 1000 Wm^{-2}on average at the Earth's surface, attenuated by absorption

in the atmosphere. The tabulated solar irradiance outside the Earth's atmosphere (AM 0), the black body spectrum, and the standard solar reference spectrum (AM 1.5G) are compared in Figure 4.2. The total incident irradiance is given by the integral of the curves and is:

$$I_{AM0} = 1366.1\ Wm^{-2} \text{and } IAM1.5G = 1000.4\ Wm^{-2} \qquad 4.1$$

For the extraterrestrial spectrum and for the reference AM 1.5G spectrum, respectively.

Absorption increases with the path length of light through the atmosphere. Fora thickness l0of the atmosphere, the path length l through the atmosphere forradiation from the Sun incident at an angle relative to the normal to the Earth's surfaceis l= l0/cos α. The ratiol/l0is called the air-mass (AM) coefficient. The standardreference spectrum in photovoltaics is designated as AM 1.5G, which corresponds to the total global (hemispherical) irradiance under specified atmospheric conditions at anangle of incidence of 48°.

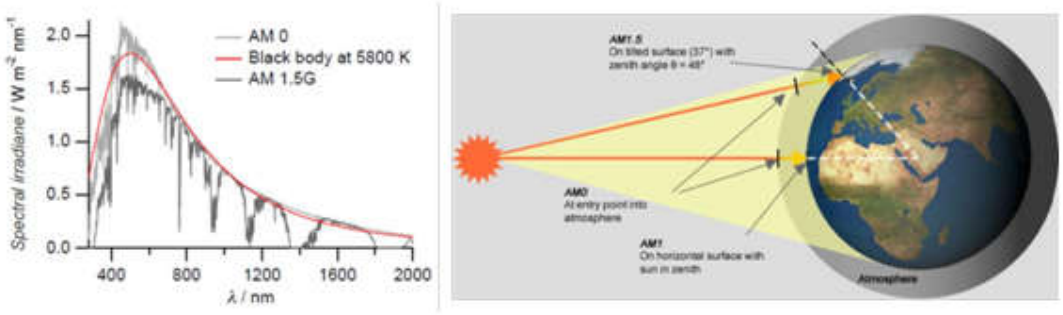

Figure 4-3 (a) Spectra of a black body absorber at T = 5800 K, the extraterrestrial AM 0 radiation, and the AM 1.5G standard solar reference radiation. Solar spectra taken from the Renewable Resource Data Center[(1)](b) Schematic of air mass[(2)]

4.3 Device Structure

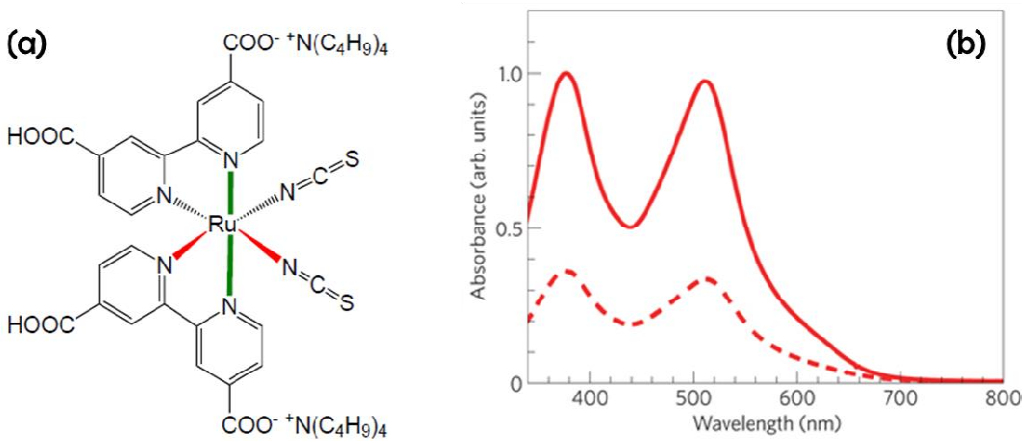

Figure 4-4(a) Molecular structure and (b) light absorbance spectrum of the sensitizer N719. [80, 82]

A schematic of a DSSC design is shown in Figure 4.3. Commonly, a colloidal TiO_2paste is deposited on a glass substrate coated with a thin transparent conducting oxide (TCO) (typically fluorine-doped tin oxide). The nanocrystalline TiO_2particles have typical sizes of 5–30 nm. The films are around 5–15 μm thick with a porosity of 60%[79]. The internal surface area of such a film is over a thousand times larger than thecompact TiO_2 layer. The sensitizing dye attached as a monolayer to this huge surface area can absorb virtually all incident light in the wavelength range of peak dye absorption. The employed dye molecule is typically a ruthenium (Ru) metal–organic complex, while the most widespread dye molecule in DSSCs is the so-called N719 (Figure 4.4)[80].The spectral absorption of the dye has a wavelength of light lying between 300 nm and 800 nm. The pores of the TiO_2film are permeated by a redox mediator, commonly the iodide/tri-iodide redox couple in an organic solvent [80]. The electrode with the mesoporous film (the photoanode) is sandwiched together with a second conducting glass substrate and a suitable sealant (e.g., hot-melt gasket). The second electrode is coated with catalytically active platinum particles for efficient reduction of oxidized redox species[81, 82-83].

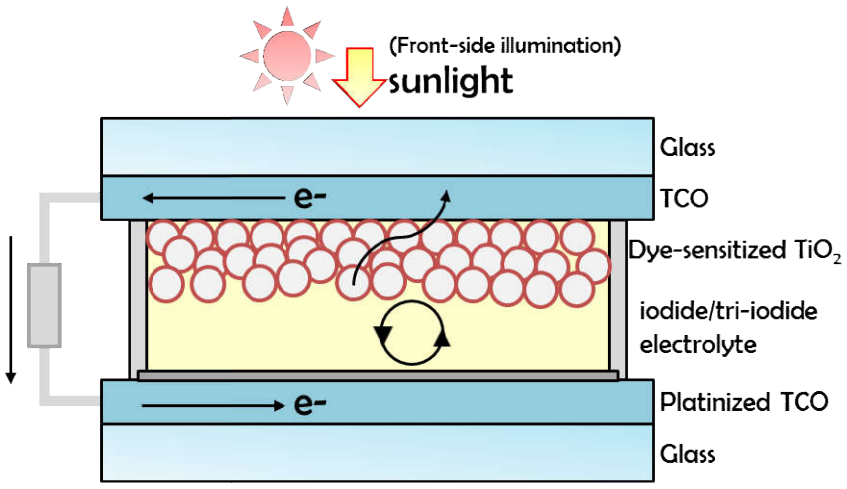

Figure 4-5Device structure of the nanostructured electrochemical DSSC

4.4 Operating Principle

The cell consists of a dye-coated semiconductor electrode and a counterelectrode arranged in a sandwich configuration, and the inter-electrode space is filledwith an electrolyte containing a redox mediator (A/A−) [81,84, 83-85].In this study, we use a polypyridine complex of Ru as the dye sensitizer, TiO_2as the semiconductor, and iodide/tri-iodide (I_2/I_3) as the redox mediator. The key reactions taking place in the dye-sensitized photoelectrochemical solar cell are shown in Figure 4.5.Light is absorbed by dye attached to the TiO_2 surface and photoexcitation of the dye forms an electronically excited state. The electron from the excited dye is injected into the conduction band of the semiconductor:

$$S + hv \rightarrow S^* \text{ (Photoexcitation)} \qquad 4.2$$

$$S^* \rightarrow S^+ + e_{cb}^- \text{ (Charge injection)} \qquad 4.3$$

The oxidized dye is subsequently reduced back to the ground state (S) by the electrondonor (A−/I−) from a redox mediator in the electrolyte:

$S^{+} + A^{-} \longrightarrow S + A$ 4.4

$S^{+} + 2I^{-} \longrightarrow S + I_2^{-}$ and $2I_2^{-} \longrightarrow I_3^{-} + I^{-}$ (Dye regeneration) 4.5

The electron in the conduction band moves through the semiconductor to a currentcollector and an external circuit. The electrons arrive at the counter electrode where they effect the reverse reaction of the redox mediator:

$A + e^{-} \longrightarrow A^{-}$ 4.6

$I_3^{-} + 2e^{-} \longrightarrow 3I^{-}$ (Electrolyte regeneration) 4.7

The net effect of this visible light irradiation is the regeneration of the dye, the redox mediator, and the driving of electrons through the external circuit. The process thus leads to direct conversion of sunlight into electricity. If only the above-cited reactions take place, then the solar cell will be stable, delivering photocurrents indefinitely. The maximum obtainable photovoltage will be the difference between the Fermi level (conduction band) of the semiconductor under illumination and the redox potential of the mediating redox couple.

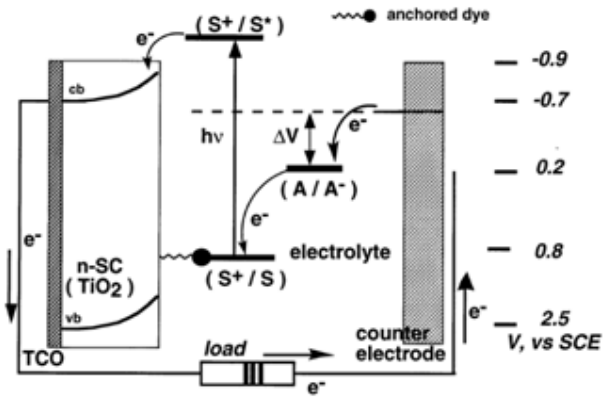

Figure 4-6 A schematic of working principles of a DSSC. [81]

Efficient photovoltaic conversion in DSSCs occurs because of a carefully balanced interplay of different kinetic processes. The kinetics of the different electron-transfer processes are summarized in **Figure 4.6**.

In the dark, the Fermi level of electrons inthe $TiO_2$is equilibrated with the redox energy level of the electrolyte ($EF_0 = E_{redox}$). When a photon is absorbed by the sensitizer (S), the excited molecule (S*) injects an electron into the conduction band (EC) of the semiconductor on a femto-to picosecond timescale (**Equation (4.2**); Photoexcitation) before the dye can relax back to its ground state:

$S^* \rightarrow S$ (Dye regeneration) 4.8

The oxidized dye (S^+) is regenerated by iodide in the electrolyte within a fewmicroseconds (Equation (4.3); Charge injection), which generally occurs more rapidly than reduction by photoinjected electrons in the TiO_2(**Equation (4.9)**; Recombination via dye).

$S^+ + ecb^- \rightarrow S$ (Recombination via dye) 4.9

The tri-iodide formed upon dye regeneration is reduced at the platinized counter electrode (Equation (4.7); Electrolyte regeneration). The additional charge in the TiO_2under illumination defines a quasi-Fermi level EFn. Electrons in the $TiO_2$are affected by two competing processes: recombination with tri-iodide in the electrolyte:

$2ecb^- + I_3^- \rightarrow 3I^-$ (Recombination via electrolyte) 4.10

and diffusion through the mesoporous $TiO_2$to the front electrode

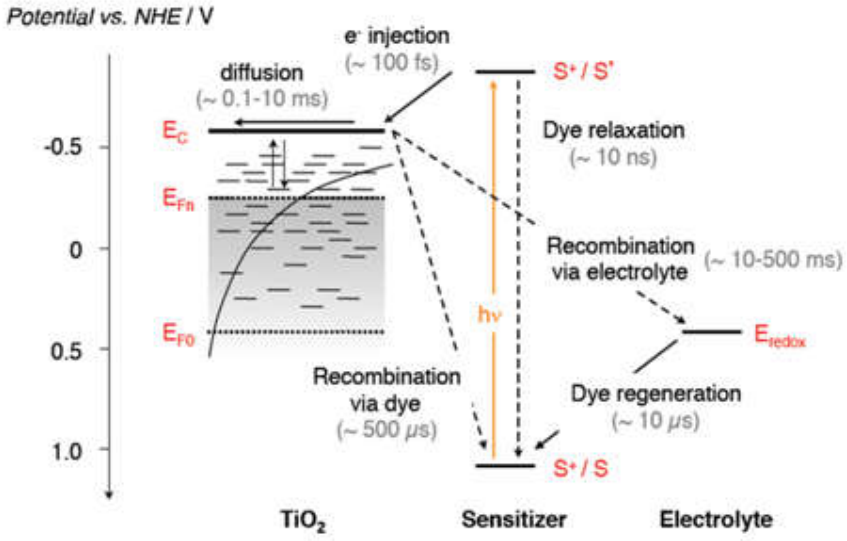

Figure 4-7 Energy diagram of a DSSC showing different kinetic processes occurring in the cell and their time scales [86]

4.5 Characterization

4.5.1 Current-Voltage Characteristics

The power conversion efficiency of a solar cell is determined from the current versus the applied voltage (I–V) characteristics under illumination[87].The I–V curve and device efficiency are reported with respect to a standard reference spectral irradiance distribution, the air-mass 1.5 global (AM 1.5G) spectrum (see Section 4.5.1). The I–V characteristics of a solar cell are well described by an equivalent electric circuit (**Figure 4.7**)[88].Under illumination, a constant photocurrent (Iph) is generated. If a forward voltage bias is applied, then a dark diode current (Idark) flows in the opposite direction. A shunt resistance (R_{shunt}) may arise from charge recombination in the photoactive layer and

induce a shunting current (I_{shunt}). The series resistance (R_{series}) includes the contact resistance at the interfaces, the bulk resistance, and the sheet resistance of the transparent electrodes. Thus, the total measured current is:

$$I = I_{Ph} - I_{dark} - I_{Shunt} = I_{Ph} - I_S\left(e^{eV/mkT}-1\right) - V+IR_{series}/R_{shunt} \quad 4.11$$

Where, Isis the diode saturation current, Vis the applied bias voltage, m is an idealityfactor (m = 1 for an ideal cell), k is the Boltzmann constant, and T is the device temperature. If we neglect the shunt and series resistances (Rshunt→ ∞, Rseries→ 0), we find simple expressions for the short-circuit current (I_{SC}) and the open-circuit voltage (V_{OC}) of the device.

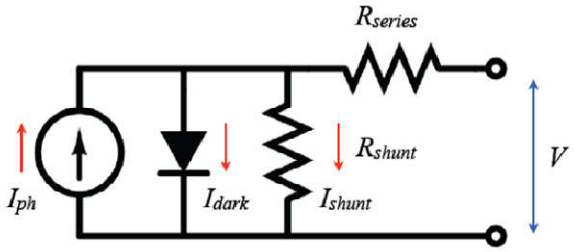

Figure 4-8 Equivalent circuit of a solar cell [83]

The short-circuit current (I_{SC}) is measured when the applied voltage is zero:

$$I^{SC} = I^{ph} \text{for } V = 0 \quad 4.12$$

The open-circuit voltage (V_{OC}) is measured when the circuit is broken or no external load is connected. In this case, there is no external current flow between the two terminals, i.e., I= 0 and V = V_{OC}.

$$V^{OC} = mkT/e \ln (I_p/I_{sh} + 1) \text{ for } I = 0 \quad 4.13$$

The maximum-power operating point defines the condition at which the power output, Pmax= ImaxVmax, of the device is maximal. The so-called fill factor (FF) is often used tocharacterize the maximum power point:

$$FF = \frac{Vmax.Imax}{Isc.Voc} \qquad 4.14$$

The FF value depends also on the shunt and series resistances. A high-performance solar cell requires a minimum Rseriesbut a maximum Rshuntin order to maximize FF. The fill factor is a value between 0 and 1 that describes the shape of the I–V curve, where a high value indicates a more preferable rectangular shape.

The solar-to-electric power conversion efficiency (η), the key parameter of the device, is calculated from the ratio of the maximum extractable power point Pmax=VmaxImaxto the incident solar power (Pin):

$$\boldsymbol{\eta = \frac{Pmax}{Pin} = \frac{Vmax.Imax}{Pin} = \frac{FF.Isc.Voc}{Pin}} \qquad 4.15$$

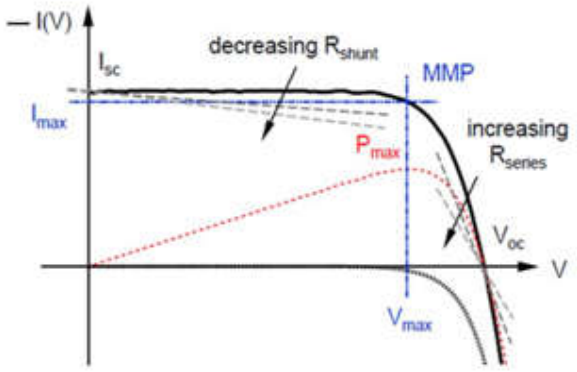

Figure 4-9 I–V curve of a typical solar cell under illumination (bold black curve) and in the dark (dashed black curve). Also shown are the power curve (dotted red), the maximum power point (MPP, blue), and the effects of the series and shunt resistances (Rseries and RShunt)

The spectral response of DSSCs is determined by measuring the monochromatic incident photon-to-current conversion efficiency (IPCE). It is customary that the IPCE be measured under short-circuit conditions. There are two principal IPCE methods: the DC and the AC method. In the DC method, monochromatic light is obtained by passing white light through a monochromator or a bandpass filter, and the photocurrent is measured. In the AC method, the monochromatic light is usually mechanically chopped, and the AC–photocurrent response is measured using a lock-in amplifier. The latter method has the advantage that white bias light can be added, so that the solar cell functions under true operational conditions. It should be noted that DSSCs have slow response times compared to solid-state photovoltaics, so a low chopping frequency must be chosen. In the DC method, the generated photocurrent may be 2–3 orders of magnitude lower than it is in full sunlight. This method will therefore only give useful results if the photocurrent increases linearly with light intensity, which is usually the case for DSSCs. A very useful test is to calculate JSC in full sunlight from the obtained IPCE spectrum:

$$Jsc = \int IPCE\ (\lambda)\ e\emptyset ph\ AM\ 1.5\ G\ (\ \lambda\ )\ d\lambda \qquad 4.16$$

Where, e is the elementary charge and ϕph, AM1.5 G is the photon flux in AM 1.5G, 100mWcm^{-2}.

The IPCE can be expressed as follows.

$$IPCE\ (\lambda) = LHE(\lambda)\varphi inj\ (\lambda)\varphi reg\eta_{cc}\ (\lambda) \qquad 4.17$$

where LHE is the light-harvesting efficiency; φinj and φreg are the quantum yields forelectron injection and dye regeneration, respectively; and ηcc is the charge collection efficiency (LHE) (1 – 10−A), with A being the absorbance of the film [84].

5 Chapter 5

5.1 Methodology

5.1.1 Literature Review

DSC is the only solar cell that separates the two functions of light harvesting and charge-carrier transport. All other conventional and OPV technologies perform both operations simultaneously. This separation opens up a vast amount of options for engineering and optimizing the different parts and functions of the cell individually.

Over the last 2 decades the amount of research in the field of DSC has increased exponentially. In this study, only literatures that are directly relevant to this project are included.

During last few years, many researchers have been studied the fabrication process and characterization of dye sensitized solar cell. They are trying to enhance the cell performance using various types of dyes, catalysts on counter electrodes, metal oxides as semiconductor etc. They also investigate the effect of electrolytes which accelerate the redox reaction inside the cell. In this section a survey of previous work on DSSC is given.

The use of dye-sensitization in photovoltaics was considered a breakthrough at the early 1990's in the Laboratory of Photonics and Interfaces in the EPFL Switzerland. By the successful combination of nanostructured electrodes and efficient charge injection dyes professor Grätzel and his co-workers developed a solar cell with energy conversion efficiency exceeding 7% in 1991 [65]. This solar cell is called the dye sensitized nanostructured solar cell or the Grätzel cell after its inventor since then an increasing interest has been shown in the fabrication and development of DSSCS.

In 2004, dye-sensitized solar cells (DSSC) were assembled by using natural dyes extracted from black rice, capsicum, erythrina, variegata flower, rosaxanthina, and kelp as sensitizers [66]. The ISC ranging from 1.142 mA to 0.225 mA, the VOC ranging from 0.551 V to 0.412 V, the fill factor ranging from 0.52 to 0.63, and Pmax ranging from 58 μW to 327 μW were obtained from the DSSC sensitized with natural dye extracts.

In 2007, some experimental data for analyzing the various dye's absorption spectra, which can be applied in the DSSC have been presents [67]. The analysis of dyes focused on the natural dyes which are extracted by the plants and compared with the chemical. The results showed that the natural dyes have the wider absorption spectra than the chemical synthesis due to the more various constituents in the natural dyes. In 2009, the performances of natural dye-sensitized solar cells assembled by using natural dyes extracted from spinach, amaranth and a mixture of them were investigated. In the sun, the Voc of cells sensitized by spinach extract was 450 mA, while those sensitezed by the mixture showed a Voc above 500 mV [68]. In 2010, twenty natural dyes, extracted from natural materials such as flowers, leaves, fruits, traditional Chinese medicines, and beverages, were used as sensitizers to fabricate DSSCs. The photoelectrochemical performance of the DSCs based on these dyes showed that the open circuit voltages (Voc) varied from 0.337 to 0.689 V, and the short circuit photocurrent densities (Jsc) ranged from 0.14 to 2.69mAcm−2[69].

5.1.2 Review of Some Previous Work Based On Tio_2Photoelectrode

Hoda Hafez et al. [70] achieved high light-to-energy conversion efficiency by applying novel TiO_2nanorod/nanoparticle (NR/NP) bilayer electrode in the N719 dye-sensitized solar cells. The short-circuit current density (Jsc), the open-circuit voltage (Voc), the fill factor (FF), and the overall efficiency (η) were 14.45 mA/cm2, 0.756 V, 0.65, and 7.1%, respectively. The single-crystalline TiO_2 NRs with length 200-500 nm and diameter 30-50 nm were prepared by simple hydrothermal methods. The dye-sensitized solar cells with pure TiO_2 NRs and pure TiO_2 NP electrodes showed only a lower light-to electricity conversion efficiency of 4.4% and 5.8%, respectively, compared with single-crystalline TiO_2 NRs. This can be attributed to the new NR/NP bilayer design that can posses the advantages of both building blocks, ie the high surface area of NP aggregated and rapid electron electron transport rate and the light scattering effect of single-crystalline NRs.

C.B. Song et al. [71] worked on DSSC using TiO_2 nanotube / nanoparticle (NT/NP) photoanodes and Cu_2SnSe_3 (CTSe) counter electrodes. They investigated the effect of the

thickness of the CTSe films on the DSSC performance. It was found that DSSC efficiencies firstly increased and then decreased with increasing the film thickness. The optimized DSSC efficiency of 3.14% was achieved at a suitable film thickness (2.9 μm). This work presents a new approach for developing low-cost alternative for expensive Pt in TiO_2-nanotube-based DSSCs.

Seulgi So et al. [72] introduced a path to the controlled construction of DSSCs based on hierarchically structured single walled, self-organized TiO_2 layers. In a first step they described a simple approach to selectively remove the inner detrimental shell of anodic TiO_2 nanotubes (NTs). This then allows controlled well-defined layer-by-layer decoration of these TiO_2-NT walls with TiO_2 nanoparticles (in contrast to conventional TiO_2 nanotubes). They showed that such defined multiple layered decorations can be optimized to build dye sensitized solar cells that (under back-side illumination conditions) can yield solar light conversion efficiencies to the extent of 8%. The beneficial effects observed can be ascribed to a combination of three factors: (1) improved electronic properties of the "single walled" tubes themselves, (2) a further improvement of the electronic properties by the defined $TiCl_4$ treatment, and (3) a higher specific dye loading that becomes possible for the layer-by-layer decorated single walled tubes.

Jiajie Fan et al. [73] studied on dye-sensitized solar cells (DSSCs) based on TiO_2nanosheets (TiO_2-NSs)/graphemenanocomposite films, and the effects of graphene on the microstructures and photoelectric conversion performance of the as-fabricated DSSC were investigated. The graphene loading clearly influences the textural properties (including specific surface areas, porosity and pore volume) and the optical absorption properties. Moreover, the charge transfer and transport versusthe charge trapping and recombination is also affected by the graphene loading. As a consequence, the photoelectric conversion efficiency of the TiO_2-NSs/graphenenanocomposite film electrodes can be improved to a great extent upon graphene loading, dependent on the loading amount of graphene. A moderate amount of graphene (<0.75 wt %) obviously enhanced the DSSC efficiency. Graphene not only reduced the electrolyte–electrode interfacial resistance and the charge recombination rate, but also enhanced the transport of electrons from the films to the fluorine doped tin oxide (FTO) substrates. Furthermore, the incorporated graphene improved the light harvesting and thus increased the number of photoinduced electrons. Also, the modified porous structures of the composite

photoanode facilitated diffusion of the electrolyte in the cell, which in turn helped to regenerate the dye, which is important for the photovoltaic response of the solar cells. However, excessive graphene loading (>0.75 wt %) largely lowered the DSSC performance. Higher graphene loading not only impaired the crystallinity of the TiO_2-NSs, but also shielded the light adsorption of the dyes and reduced the number of photogenerated electrons.

JiaopingCai et al. [74] reported a new titanium dioxide (TiO_2) slurry formula for the fabrication of TiO_2photoanode for use in dye-sensitized solar cells(DSSCs). The prepared TiO_2photoanode featured a highly uniform mesoporous structure with well-dispersed TiO_2nanoparticles. The energy conversion efficiency of the resulting TiO_2 slurry-based DSSC was ~63% higher than that achieved by a DSSC prepared using commercial TiO_2slurry. Subsequently, the incorporation of acid-treated multi-walled carbon nanotubes(CNTs) into the TiO_2slurry was examined. More specifically, the effect of varying the concentration of the CNTs in this slurry on the performance of the resulting DSSCs was studied. The chemical state of the CNTs-incorporated TiO_2photoanode was investigated by Fourier transform infrared spectroscopy and X-ray photoelectron spectroscopy. A high energy conversion efficiency of 6.23% was obtained at an optimum CNT concentration of ~0.06 wt%. The obtained efficiency corresponds to a 63% enhancement when compared with that obtained from a DSSC based on commercial TiO_2slurry. The higher efficiency was attributed to the improvement in the collection and transport of excited electrons in the presence of the CNTs.

5.2 TiO_2 DSSC Preparation Process

A typical Dye Sensitized solar cell manufacturing process includes:

Step 1: Identify the conducting side of a tin oxide-coated piece of glass by using a multimeter to measure resistance. The conducting side will have a resistance of 20-30 ohms.

Step 2: With the conducting side up, tape the glass on three sides to the center of a spill tray using one thickness of tape. Wipe off any fingerprints or oils using a tissue wet with ethanol.
Opposite sides of tape will serve as a spacer (see below) so the tape should be flat and not wrinkled. The third side of tape gives an uncoated portion where an aligator clip will be connected

Step 3: Add a small amount of titanium dioxide paste and quickly spread by pushing down and across with a microscope slide before the paste dries. The tape serves as a 40-50 micrometer spacer to control the thickness of the titanium dioxide layer if you push down.

Step 4: Carefully remove the tape without scratching the TiO_2 coating. Leave the removed tape in a spill tray for disposal.

Step 5: Heat the glass on a hotplate in a hood for 10-20 minutes. The surface turns brown as the organic solvent and surfactant dries and burns off to produce a white or green sintered titanium dioxide coating. (Note: this requires a plate that gets quite hot.) Allow the glass to slowly cool by turning off the hotplate. The sample will look quite similar before and after heating; you only know it is done if you have observed the darkening stage along the way.

Step 6: Immerse the coating in a source of anthocyanins, such as raspberry juice. The raspberry juice may be obtained from frozen raspberries. (Blackberries, pomegranate seeds, and Bing cherries can also be used.) The white TiO_2 will change color as the dye is absorbed and complexed to the Ti(IV).

Step 7: Rinse gently with water to remove any berry solids and then with ethanol to remove water from the porous TiO_2. The ethanol should have evaporated before the cell is assembled.

Step 8: Pass a second piece of tin oxide glass, conducting side down, through a candle flame to coat the conducting side with carbon (soot). For best results, pass the glass piece quickly and repeatedly through the middle part of the flame.

Step 9: Wipe off the carbon along the perimeter of three sides of the carbon-coated glass plate using a dry cotton swab.

Step 10: Assemble the two glass plates with coated sides together, but offset so that uncoated glass extends beyond the sandwich. Do not rub or slide the plates. Clamp the plates together with binder clips.

Step 11: Add a drop of a tri-iodide solution to opposite edges of the plate. Capillary action will cause the KI3 solution to travel between the two plates. (The KI_3 electrolyte solution consists of 0.5 M KI and 0.05 M I_2 in anhydrous ethylene glycol.) The solution can corrode the alligator clips in the next step so wipe off an excess.

5.3 Surface Structure

Two opposing characteristics - film porosity and effective surface area – are the performance defining criteria for DSC. The photo-generated current increases with the increment of surface area, while it decreases with the increase of porosity. Porosity is a measure of the void spaces in a material, and is defined as the fraction of the volume of empty spaces over the total volume, normally represented as a percentage between 0~100. Photo-generated current from the solar cell increases with the increase of surface area due to the availability of more anchoring site for the dyes. An increasing porosity causes to generate less current due to the reduction in the mass of TiO_2 per square centimeter of film as well as the effective TiO_2 surface per square centimeter. Less surface area leads to a lower density of dye molecules adsorbed. Hence, less porosity is desirable.

However, the charge carriers diffuse slowly in the electrolyte in the presence of small pores. In a 4nm diameter pore, the dye molecules absorbed on the pore walls occupy 3nm of it (molecular diameter of dyes ~1.5nm). An aperture of only 1nm is available for the diffusion of the electrolyte, which is close to the size of the tri-iodide ion. Obviously, the transport kinetics is also affected by other parameters, like the electrolyte solvent viscosity and the iodine concentration.[89]

The size, shape, and crystal structure of the TiO_2 nanoparticles depend on the method of preparation of the paste.[90] The porosity is also a function of the annealing temperature profile. The average pore size increases from 15nm to 20nm with an increasing temperature from 400°C. However, with annealing temperatures above 500°C this trend becomes stable with no change in the pore-size distribution.[89] An annealing temperature study from 150°C to 450°C shows an increasing J_{SC} for films annealed at higher temperature, due to higher porosity. This is attributed to the increase of diffusion coefficient and carrier lifetime with increasing temperature.[91]

TiO_2 nanoparticle size is another key parameter for DSC. With increasing particle size electron diffusion coefficient increases due to the decrease of surface area and the structure of grain boundaries. On the other hand, electron recombination lifetime decreases with particle size increase. Thus, a small particle size would be favorable for DSC applications. However, charge injection efficiency is lowered with the decrease of the particle size due to reduced diffusion length. Hence, an optimization in the particle size is the requirement.[92]

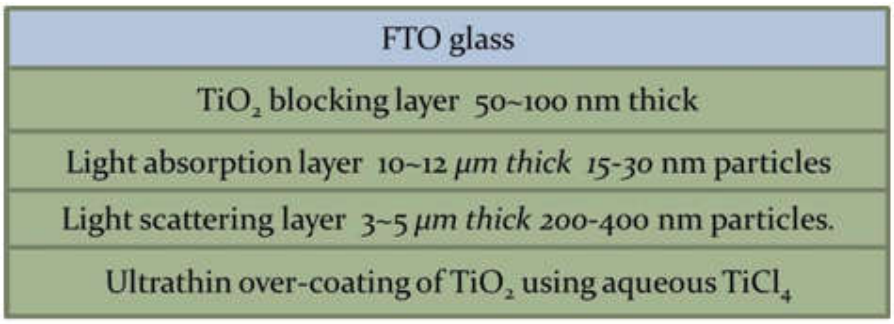

Figure 5-1 TiO_2 structure of DSC for optimum performance

The typical film thickness for DSC is 5–20μm with the TiO_2 mass of about 1–4 mg/cm^2. An optimum surface area of the sintered TiO_2 colloid is 75m^2/g and a porosity of 50–65%.[93] For a 10-15 μm thick titania film the effective surface area is increased over a thousand times, which is the beauty of the mesoscopic structure, allowing for a dense monolayer of adsorbed sensitizer. The nano-particles have an average size of 15-30nm. HRTEM measurements shows that the preferred orientation is (1 0 1) due to its lower surface energy, followed by (1 0 0) and (0 0 1). [94]

5.4 Semiconductor Thickness

For DSC, the thickness of the TiO_2 layers directly controls the photon adsorption. For single-layer electrodes (20nm particles) a small but linear decrease in the open-circuit voltage (V_{OC}) is observed with increasing thickness. However, thickness response of the short-circuit current density (J_{SC}) depends on the viscosity of the electrolyte. A low viscosity electrolyte can support higher photocurrent generated from thick nanocrystalline-TiO_2 layer, hence the current will exhibit a linear rise. However, for high viscosity electrolyte a peak in the current is observed and after that, it decreases. The thickness dependence is also a function of particle size and surface structure. For example, optimal thickness for 20nm particles is half of that obtained for the 42nm particles. [95]

5.5 Light Scattering Layer

One limitation of the sensitizing dyes is their poor performance in the near infra-red spectrum of light. A way of improving this is - by introducing an additional light scattering layer of larger titania particles. These can be mixed with or screen-printed on top of thefilm of 15-30nm sized TiO_2 particles. This allows the scattered photons to be contained in the film by means of multiple reflections, increasing their optical path length substantially beyond the film thickness. Consequently, the solar light absorption is enhanced, especially in the red to near-IR regions. With the use of 200-400nm sized anatase particles as light-scattering centers, an increment of the J_{SC} by 3-4 mA/cm^2 was observed for N719-based DSCs because of the enhanced light absorption.

Moreover, approximately 4% loss occurs because of the reflection of incident light on the glass substrate. This can be partially overcome by introducing an anti-reflecting film, which can also act as a UV cut-off filter.[99]

5.6 Blocking Layer

Charge recombination is one of the main reasons of lower current for DSC. Recombination occurs at both Electrode/Electrolyte and TiO_2/Electrolyte interface. A compact blocking layer of TiO_2 by RF sputtering[96] or spray pyrolysis[97] between the conducting electrode and the nanocrystalline TiO_2 layer can effectively prevent the recombination at electrode/electrolyte interface. Introduction of this layer prevents electrolyte from reaching the electrode (increases J_{SC}) and also enhance electron transport from nanocrystallinetitania to the electrode (increases V_{OC}). This blocking layer is absolutely necessary for planar organic dyes, while ruthenium based sensitizers can perform this anode insulation themselves against recombination losses.[98]

A rather cost effective and easier way of incorporating this blocking layer is through hydrolysis of $TiCl_4$. $TiCl_4$ treatment on FTO substrate is found to suppress the dark current, shifting its commencement by some hundred millivolts. This is due to a positive shift in the conduction band edge of highly doped SnO_2 by about 0.5 V which results in a higher electron density in the FTO substrate.[99] This blocking layer can also be made of other metal-oxides such as ZnO or Nb_5O_2.[100]

5.7 Doping

Doping of TiO_2 has been an important approach in band gap engineering to change the optical response of semiconductor photocatalysts. The main objective of doping is to induce a bathochromic shift, i.e., a decrease of the band gap or introduction of intra-band gap states, which results in the absorption of more visible light. Doping may lead to photocatalytic systems that exhibit enhanced efficiency [112]. It is desirable to maintain the integrity of the crystal structure of the photocatalyst while changing its electronic structure by doping. It is easier to replace Ti4+ in TiO_2 with a cation than to substitute O^{2-} with another anion because of the difference in the charge states and ionic radii [113].

Nanomaterials show a higher tolerance to structural distortion than bulk materials due to their inherent lattice strain. As a result, the surface modification of TiO_2 nanoparticles appears to be more beneficial than the modification of bulk TiO_2 [114].

5.8 Doping with transition metal cations

Transition metal ions can provide additional energy levels within the band gap of a semiconductor. Electron transfer from one of these levels to the conduction band requires lower photon energy than in the situation of an unmodified semiconductor. TiO_2 has been doped with many different transition metals [72–86]. Grätzel et al. [73] studied the effect of doping TiO_2 with transition metals such as Fe, V, and Mo by electron paramagnetic resonance. Choi et al.[74] carried out a systematic investigation of the photoreactivity of TiO_2 doped with 21 different metal ions. Dopants such as Fe(III), Mo(V), Ru(III), Os(III), Re(V) and V(V) substantially enhanced the photochemical reactivity of TiO_2 for the oxidation of $CHCl_3$ and reduction of CCl_4.

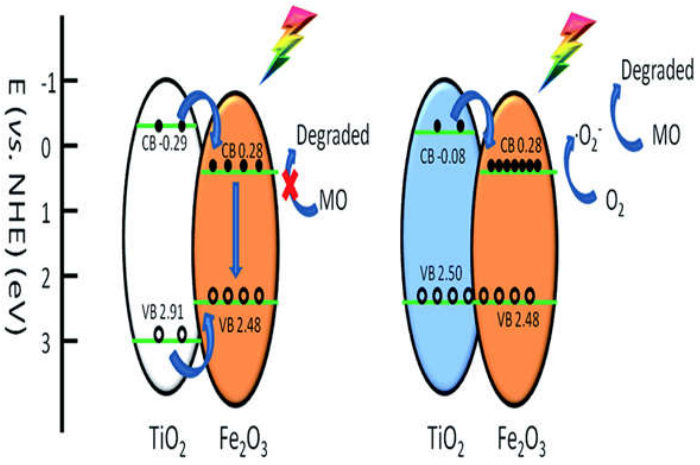

Figure 5-2 Fe_2O_3 doping at TiO_2 nanoparticles process

Enhancing the rate of photoreduction by doping a semiconductor with metal ions can produce a photocatalyst with an improved trapping-to-recombination rate ratio. However, when metal ions or oxides are incorporated into TiO_2bydoping, the impurity energy levels formed in the band gap of TiO_2 can also lead to an increase in the rate of recombination

between photogenerated electrons and holes. Photocatalytic reactions can only occur if the trapped electron and hole are transferred to the surface of the photocatalyst. This means that metal ions should be doped near the surface of the photocatalyst to allow efficient charge transfer.In the case of doping at a high concentration, metal ions can behave as recombination centers. Joshi et al. [75] reported the adverse effect of doping TiO_2 with transition metal ions on photocatalytic activity because of the formation of localized d-states in the band gap of TiO_2. Localized d-states act as trapping sites that capture electrons from the conduction band or holes from the valence band.

From a chemical point of view, TiO_2 doping is equivalent to the introduction of defect sites like Ti3+ into the semiconductor lattice, where the oxidation of Ti3+ species is kinetically fast compared with the oxidation of Ti4+. The differences in photoactivity derive from the change in the diffusion length of the minority carriers [76]. For optimal e–/h+ separation, the magnitude of the potential drop across the space-charge layer should not fall below 0.2 V [77]. The dopant content directly influences the rate of e–/h+ recombination by the equation: $W = (2 \varepsilon\varepsilon_o V_s / eN_d)$, where W is the thickness of the space-charge layer, ε is the static dielectric constant of the semiconductor, εo is the static dielectric constant in a vacuum, Vs is the surface potential, Nd is the number of dopant donor atoms, and e is the electron charge [78]. As the concentration of the dopant increases, the space-charge region becomes narrower and the electronhole pairs within the region are efficiently separated by the large electric field before recombination. However, when the concentration of doping is high, the space-charge region is very narrow so the penetration depth of light into TiO_2 greatly exceeds the width of the space-charge layer. Therefore, the rate of recombination of photogenerated electron-hole pairs in the semiconductor increases because there is no driving force to separate them. Consequently, there is an optimum concentration of dopant ions where the thickness of the space-charge layer is similar to the depth of light penetration. Xin et al. [79] reported enhanced photocatalytic activity of TiO_2 containing a low doping concentration of Fe3+ ($Fe/Ti \leq 0.03$ mol) and reduced photocatalytic activity at higher concentrations. Li et al. [80] prepared zero-valent Fe-doped TiO_2nanorods by an in situ reduction route using templareTiO_2nanorods that were pre-synth- esized using a traditional alkaline hydrothermal method. The photocatalytic degradation of acetic acid and formaldehyde by the doped nanorods was investigated under irradiation with UV light.

The photoactivity of the Fe-doped TiO_2nanorods was much higher than that of Degussa P-25. Periyasami et al. [81] synthesized pure and Fe-doped nanocrystalline TiO_2 by combining a sol-gel technique with hydrothermal treatment. Doping with Fe caused a significant shift in absorption towards the visible region compared with that of Degussa P-25 and pure TiO_2. The photocatalytic activity of TiO_2 doped with Fe exceeded those of undoped commercial and synthesized pure TiO_2 for the oxidative degradation of 2,4,6-trichlorophenol.

5.9 Experimental DSSC Preparation

5.9.1 Materials

Materials used in this experiment were Flourine Tin Oxide (FTO) coated glass plate (Dyesol, Australia), TiO_2 (Degussa P25, USA) , Fe2O3, Titanium IV Isopropxide (TTIP) (Merck, Germany),Polyoxethylene (10) octylphenyl ether (Triton X-100) (Merck, Germany), Acetlacetone (BDH, UK), Acetone (BDH, UK), Ethanol (BDH, UK), Deionized water, Dye extracted from red amaranth (Amaranthusgangeticus, local Bangladeshi name lalshak) in our lab, Carbon from flame tip, Potassium Iodide and Iodine.

5.9.2 Preparation of Fe_2O_3 Doped TiO_2 Paste

TiO_2 , Degussa P25 powder doped with five ratios of Fe_2O_3 like 1.96g of Degussa P25 with 0.04g of Fe_2O_3, 1.92g of Degussa P25 with 0.08g of Fe_2O_3 , 1.88g of Degussa P25

with 0.12g of Fe_2O_3, 1.84g of Degussa P25 with 0.16g of Fe_2O_3,1.80g of Degussa P25 with 0.20g of Fe_2O_3. Which means Fe_2O_3 is doped at 2%, 4%, 6%, 8% and 10% ratio of total mixture with Degussa P25. We named three mixtures as No.1, No. 2, No. 3, No 4, and No. 6. respectively.

The three mixtureswere deposited in three beakers mixed with 0.1 M, 0.2 mL of acetylacetone, 0.2 mL polyethylene glycol, During vigorous stirring10 ml mixture of water and ethanol (1: 1 vol%) was added and 0.8 mL nonionic surfactant triton X-100. The mixture was well mixed with the help of a glass rod and then kept in an ultrasonic bath for half an hour for the production of suspension with a consistency of a thick paint produced. The mixture then placed on the magnetic stirrer for 40-60 minutes. The prepared paste was coated on FTO glass with surface resistance of 10-30 ohms by using doctor blade technique.

Before this process, first the sample FTO slides are cleaned by brush with de-ionized water and washed by methanol as mechanical scrubbing.Then slides were cleaned in firstly in a methanol solution for 10 minutes and then in acetone for 10 minutes.

Elements	Role	Amount
Degussa P25,Titanium Di Oxide (TiO_2)	Starting Material	No.1#1.96g, No.2#1.92g, No.3#1.88g No.4#1.84g No.5#1.80g
Ferric Oxide (Fe_2O_3)	Doping Material	No.1#0.04g No.2#0.08g No.3#0.12g No.4#0.16g No.5#0.20g
Ethanol (CH_3CH_2OH)	Solvent	5 ml
Acetylacetone	Stabilizer	0.2 ml

Deionized Water (H_2O)	Solvent	5 ml
Triton X-100	Stabilizer	0.8ml

Table 2 Elements of Fe_2O_3 doped TiO_2 solution

Figure 5-3 Exact Weight Measurement of solid Materials

5.9.3 Magnetic Stirring of the Solution

Taking all elements in a 100ml beaker according to the measured amount themagnetic stirring was done with 78-1 MAGNETIC STIRRER HOTPLATE for 2hr at 25oC and then the solution was allowed to aged for 2 hr in room temperature.

Figure 5-4Magnetic Stirring of the solution at**MAGNETIC STIRRER HOTPLATE**

5.9.4 Controlling the Thickness

The thickness of the coating was controlled using the simplest and most widely used doctor-blade method. With this technique, the thickness of the paste layer is determined by the thickness of a spacer placed on both sides. Using the Scotch tape which has a thickness of 20 µm, 2 Layer = 40 µm, 3 Layer = 60 µm, 4 Layer = 80 µm and 5 Layer = 100 µm, with the conductive side facing up, apply two parallel strips of tape on the edges of the glass plate.

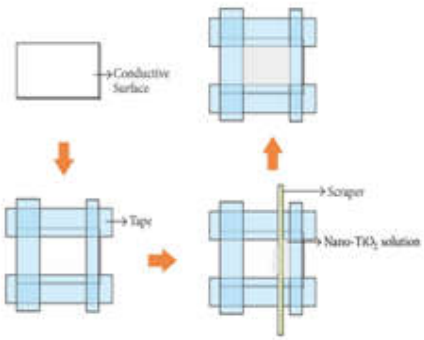

Figure 5-5 Coating of the FTO glass slide by Doctor Blade Technique

The area of the middle of the glass is uncovered and where the TiO_2 paste will be deposited.

After depositing the paste remove the scotch tape. Two bare edges masked by the tape will give then room for future sealing and electrical contacts.

After each coating procedure the deposited electrodes are put into an dryer for raising the Temperature to complete the ageing process.

Figure 5-6 Drying and Ageing at 60°C in drying oven hot air dryer DHG-9130/130L stainless steel lab machine

5.9.5 Annealing Electrode for Densification

The electrodes were annealed at temperature ranging from 0 ºC – 450 ºC (0 ºC,50 ºC, 100ºC, 150 ºC, 200 ºC, 250 ºC, 300 ºC, 350 ºC, 400 ºC, 450 ºC) for half an hour with the help of a furnace. After the annealing was completed, the TiO_2 coated conductive glass was allowed to cool slowly at room temperature and then the TiO_2 coated glass plate was prepared for dye soaking.

Figure 5-7 Air annealing of samples with machine DTLCSP C-1000

After annealing the Fe_2O_3 doped TiO_2 DSSC films, furnace is then left to cool down to ambient temperature again. Then it is kept for 24 hours for making it stable and thus the electrode preparation process has accomplished and samples are ready for experimental testing.

Figure 5-8 Prepared Electrode samples for testing

5.9.6 Extraction of Natural Dye and Staining The Electrode

Red amaranth leaves were collected from local market and then washed and kept them some times for dried. 100 g of leaves were weighted and crushed in a mortar and pastel adding 50 mL of solvent. The extracted dye was filtered three times with a cotton cloth and stored in a dark bottle covered with aluminium foil paper. The TiO2 coated glass plate was soaked in dye and was kept at a dark place. The glass plate was washed by distilled water and then ethanol and dried in air for 30 minutes.

Figure 5-9 Red Amaranth (In Bengali 'lalshak')

Figure 5-10Dye Paste Prepared from Red Amaranth

(a)

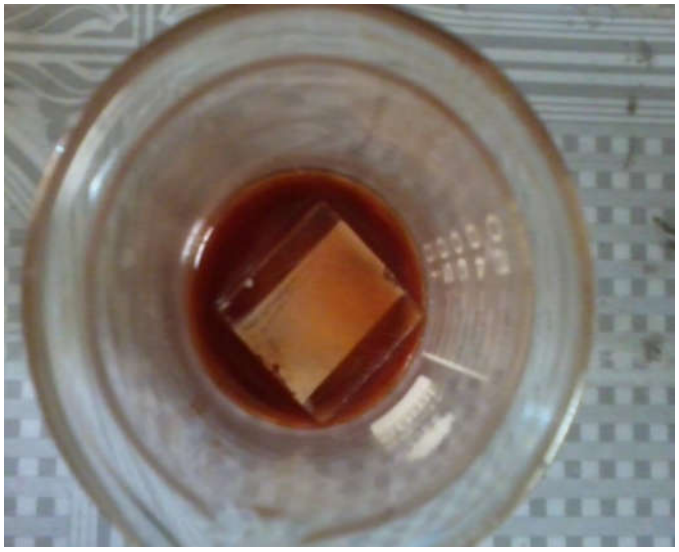

(b)

Figure 5-11 Prepared dye is (a) spilling on the photo electrode surface and (b) Photoelectrode is in dye

5.9.7Preparing counter electrode and Electrolyte

The counter electrode was prepared by exposing the conductive side of an ITO coated glass to candle light for 2-3 minutes which leaves a dark shade of carbon on the glass.

To prepare electrolyte 8.3 g of 0.5 M potassium iodide and 1.27 g of 0.05 M iodine was mixed in ethylene glycol until it is 100 mL. The solution was stored in a black bottle and was used when necessary.

Figure 5-12 Prepared Counter Electrode made by tip of Flame

Figure 5-13Electrolyte is pouring in the prepared DSSC

5.9.8 Assemblingthe Cell

Electrode and counter electrode were combined together keeping TiO2 paste coated surface and the carbon coated surface face to face. 2/3 drops of electrolyte solution was given in the contact of two glasses and by the capillary action the electrolyte was uniformly distributed throughout the stained TiO2 film. Excess electrolyte from the exposed area of the glass was wiped off by using cotton or tissue. The complete cell was

then taken to sunlight for harvesting energy.

5. 9.9 Measuring electric properties

Electrical properties were measured by using two digital multimeter keeping the cell in sunlight of approximately 100 mW/cm2 illumination. Current and voltage were measured by multimeters changing with resistance with the help of a variable resistor. Based on I-V curve, the fill factor (FF) was defined as

$FF \ (=I\max \times V\max)/(I\ sc \times Voc)$
where

I max and Vmax are the photocurrent and photovoltage for maximum power point(Pmax)
.
$I\ sc$and $Voc$are the short-circuit photocurrent and open-circuit photovoltage respectively. The overall energy conversion efficiency (η) is defined as

$(\eta = I\ sc \times Voc \times FF)/ Pin$
where

Pin is the power of incident light.

5.9.10 Thickness Measurement

In case of solar cells, the coating thickness of the optical materials and its uniformity has to be monitored. The layer thickness is influencing the efficiency and, in addition, the surface color, defining the appearance. Hence, measuring the right thickness and composition of active layers is important for determining the solar cell performance. Being too thin can affect efficiency and durability, while being too thick can increase cost. The wrong composition can drastically decrease efficiency and manufacturing yield. Profilometer is used to measure the surface thickness of the film. Profilometer is a measuring instrument used to measure a surface's profile, in order to quantify its roughness. It is a device similar to a phonograph that measures a surface as the surface is moved relative to the contact profilometer's stylus, this notion is changing with the emergence of numerous non-contact profilometery techniques.

6 Chapter 6:
Results & Discussions

6.1 Effects of Fe2O3 Doping on TiO2 Photo Electrode

Photo electrode (PE) of dye-sensitized solar cell (DSSC) can be prepared with different materials and methods. Here we prepared six samples of different doping concentration ratio and one for no doping. The photovoltaic performances of the DSSC based on different doping concentration for photo electrode are shown in **Fig. 6.1**.

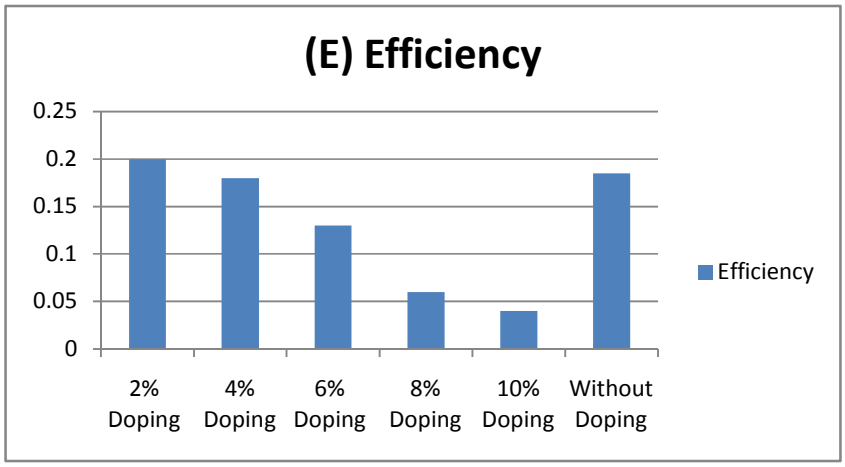

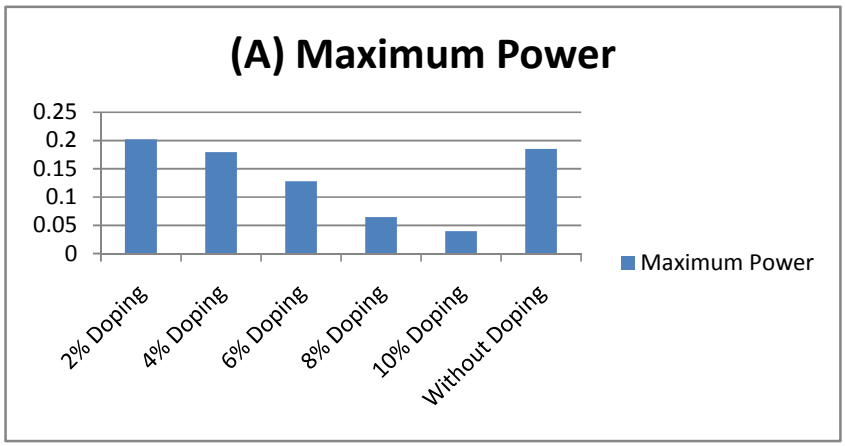

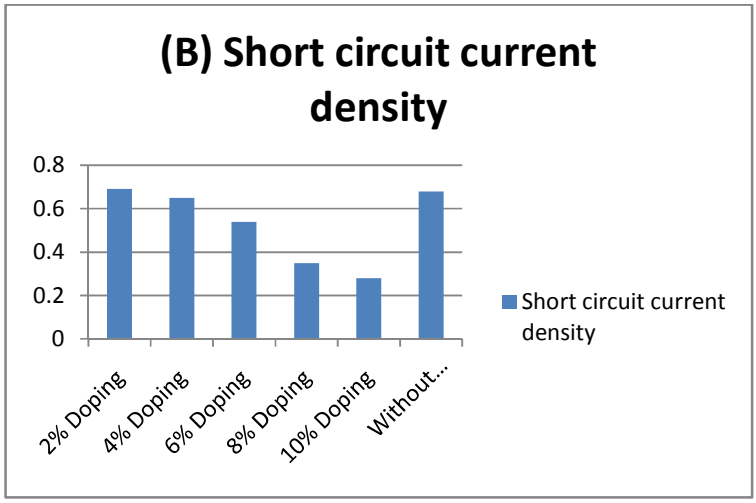

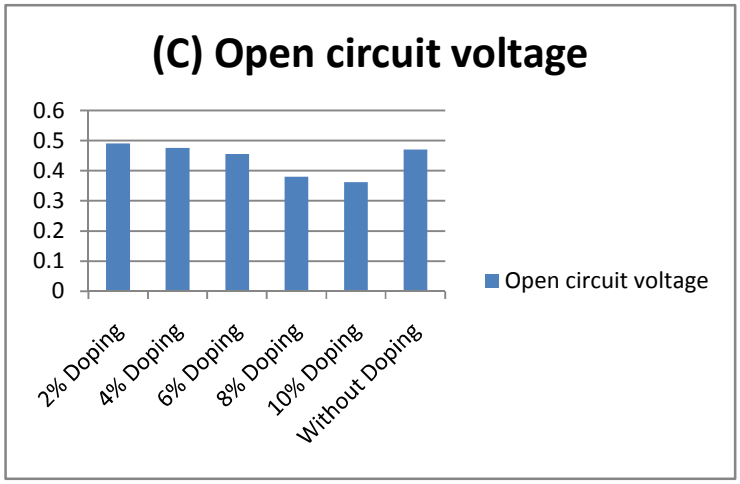

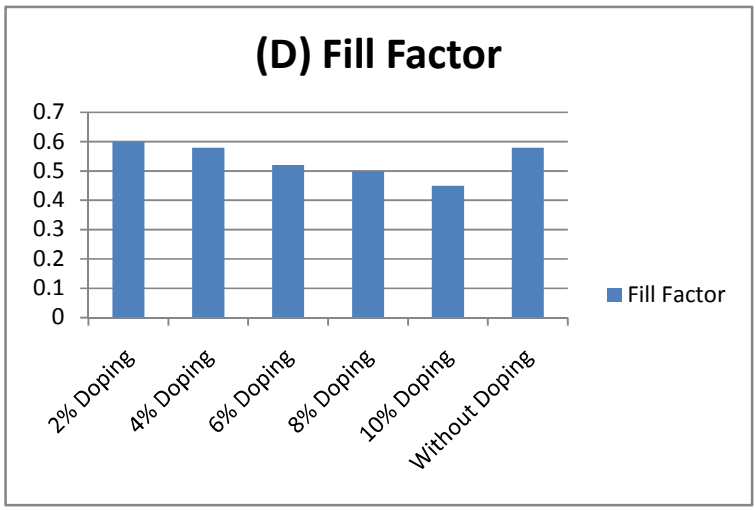

Figure 11 Photovoltaic characteristic parameters of the DSSC with different doping concentration ratio for photo electrode (A) Maximum Power (B) Short circuit current density (C) Open circuit voltage (D) Fill Factor (E) Efficiency

Fig. 6.1.Photovoltaic characteristic parameters of the DSSC with different doping concentration ratio for photo electrode (A) Maximum Power (B) Short circuit current density (C) Open circuit voltage (D) Fill Factor (E) Efficiency .

Open circuit voltage (Voc), short circuit current density (Jsc) and maximum power, Fill factor (FF), Efficiency(η) are obtained for each DSSC are summarized in **Table 6.1**. Amongst the different doping ratio of photo electrode the DSSC with 2-4% Fe2O3 doped TiO2 photoelectrodehas shown maximum open circuit voltage 0.490 V and short circuit current density 0.69 mA/cm2 resulting maximum power density 0.338mW/cm2. This indicates that Fe2O3 doping concentration of 2-4% has strong efficiency enhancing activity and stability proved.

Table 6.1. Photovoltaic parameters of the DSSC for different thickness of Fe2O3 doped TiO_2 film.

Sample Number	**Thickness(μm)**	**V_{oc} (V)**	**Jsc [mA/cm2]**	**P max [mW]**	**F.F.**	**η %**
1 (2% Doping)	20	.491	.69	.202	.60	.20
2 (4% Doping)	20	.475	.65	.179	.58	.18
3 (6% Doping)	20	.455	.54	.128	.52	.13
4 (8% Doping)	20	.380	.35	.065	.50	.06
5 (10% Doping)	20	.362	.28	.040	.45	.04
6 (Without Doping)	20	.470	.68	.185	.58	.185

6.2 Effects of Doping Concentration by varying Thickness of Fe2O3 doped TiO2 Film on Photo Electrode

In case of solar cells, the coating thickness of the optical materials and its uniformity has to be monitored. The layer thickness is influencing the efficiency and, in addition, the surface color, defining the appearance. Hence, measuring the right thickness and composition of active layers is important for determining the solar cell performance. Being too thin can affect efficiency and durability, while being too thick can increase cost. The wrong composition can drastically decrease efficiency and manufacturing yield.

Profilometer is used to measure the surface thickness of the film. Profilometer is a measuring instrument used to measure a surface's profile, in order to quantify its roughness. It is a device similar to a phonograph that measures a surface as the surface is moved relative to the contact profilometer's stylus, this notion is changing with the emergence of numerous non-contact profilometery techniques.

6.2.1 Thickness Testing

Thickness measurement was done at Institute of Electronics, Atomic Energy Research Establishment (AERE), Savar, Dhaka. Stylus Surface Profilometer, Model: Detak-150 was used for the testing. Substrates with layer of 1,2,3,5 & 8 times were experimented to observe the variation of thickness in the substrates regarding layer increment.

Figure 6.2: Stylus Surface Profilometer, Model: Detak-150

Table 6.2. Photovoltaic parameters of the DSSC for different thickness of 2% Fe2O3 Doped TiO2 film.

Sample Number	**Thickness(µm)**	**Voc (V)**	**Jsc [mA/cm^2]**	**P max [mW]**	**F.F.**	**η %**
1	20	.491	.68	.201	.60	.20
2	30	.490	.67	.200	.61	.20
3	40	.442	.45	.115	.58	.11
4	50	.390	.38	.077	.52	.07
5	60	.376	.31	.058	.50	.06
6	70	.352	.30	.052	.50	.05
7	80	**Coating was not Stable**				

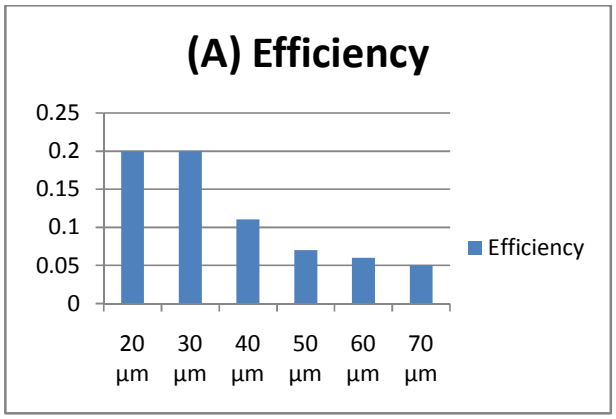

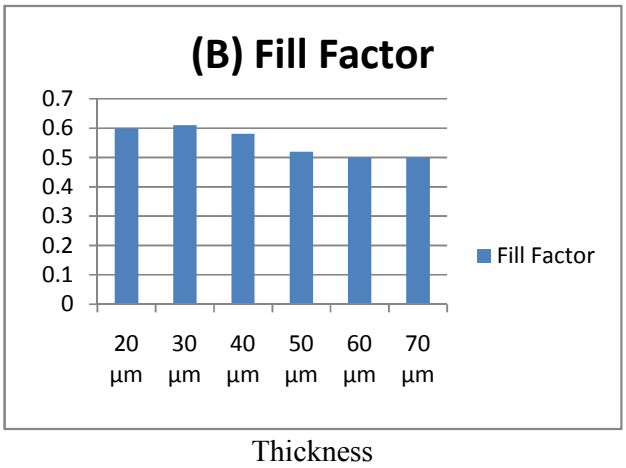

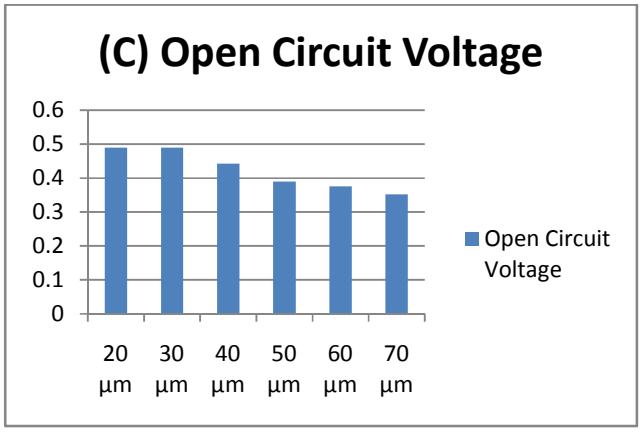

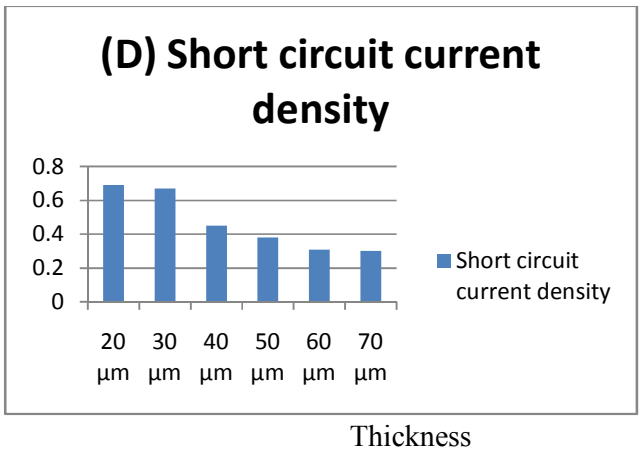

Fig.6. 3.Photovoltaic characteristic parameters for the DSSC with various thickness of 2% Fe2O3 doped TiO2film (A)Efficiency (B) Fill factor (C) Open circuit voltage (D) Short circuit current density.

Table 6.3. Photovoltaic parameters of the DSSC for different thickness of 4% Fe2O3 Doped TiO2 film.

Sample Number	**Thickness(µm)**	**V_{oc} (V)**	**Jsc [mA/cm2]**	**P max [mW]**	**F.F.**	**η %**
1	20	.475	.65	.179	.58	.18
2	30	.463	.61	.161	.57	.16
3	40	.449	.47	.112	.53	.11
4	50	.370	.36	.065	.49	.06
5	60	.356	.32	.052	.46	.05
6	70	.344	.29	.045	.46	.04
7	80	**Coating was not Stable**				

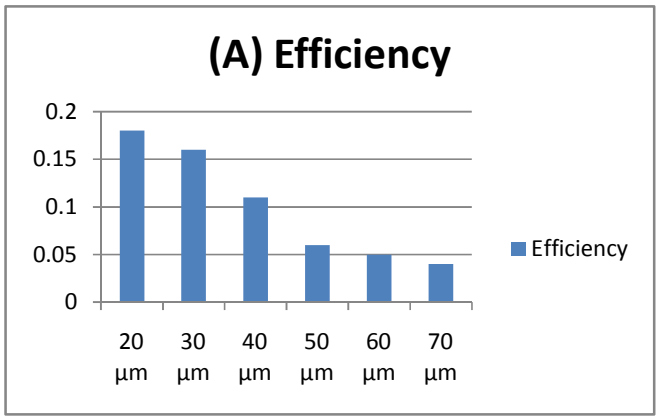

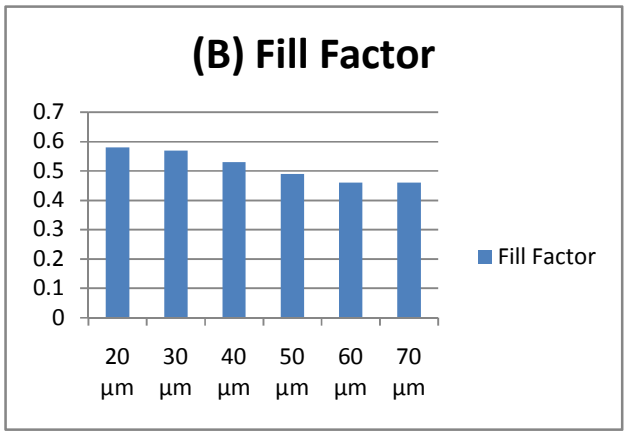

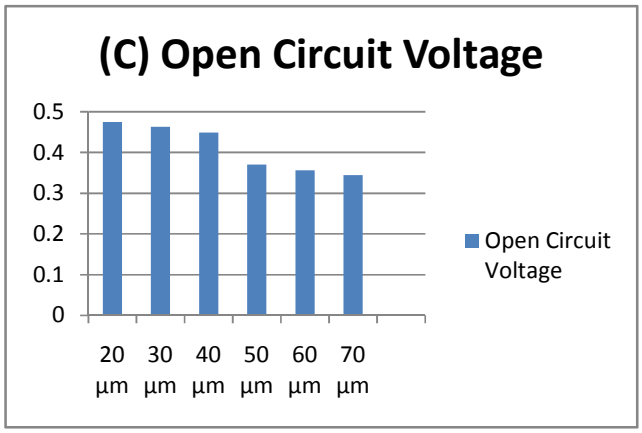

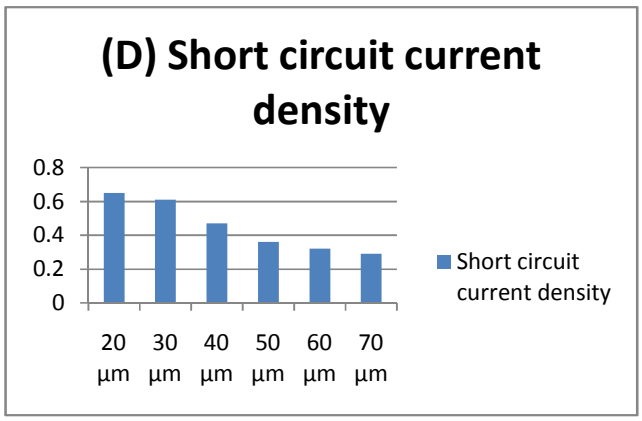

Fig.6.4. Photovoltaic characteristic parameters for the DSSC with various thickness of 4% Fe2O3 Doped TiO2 film (A)Efficiency (B) Fill factor (C) Open circuit voltage (D) Short circuit current density.

So, The maximum photovoltaic conversion efficiency was achieved for a 2%-4% Fe2O3 doped TiO2 film thickness of 20-30 µm.

6.3 Discussion

It is been observed that a huge improvement in layer thickness with each deposition. For single deposition of Fe2O3 doped TiO2 the layer thickness was found 10 µm, which is quiet regardable. At 2,3,5& 8 times deposition, the layer thickness improved significantly,highest 80 µm which is almost 8 times greater than the thickness found for 1 time deposition.

The effect of the doping on TiO2 photoelectrode on the performance of the DSSCs was investigated. The Fe2O3 doped TiO2 film can not only improve adherence of TiO2 to FTO and provide a larger TiO2/FTO contact area, but also effectively increase the electron recombination by minimising the direct contact between the redox electrolyte and the conductive FTO surface.

Nanostructured semiconductor films are the framework of DSSC photoanodes. The photoanode serves dual functions as the support for sensitizer loading and transporter of photo-excited electrons from sensitizer to external circuit. Therefore, a large surface area is necessary to ensure high dye loading.Moreover, a fast charge transport rate is required to ensure high electron collection efficiency. These two properties are the defining characteristics of an ideal photoanode.

In a DSSC, a 10 mm thick film composed of a three-dimensional (3D) network of randomly
dispersed spherical TiO2 nanoparticles is typically employed as a photoanode. Although the large surface area (50 m2/g) of nanoparticles enables a high dye loading capacity, the disordered
network with numerous grain boundaries weakens electron mobility and results in slow transport and recombination of photoexcited electrons. This greatly restricts the overall efficiency of such devices .

The dye extraction temperature plays a major role in determining the charge-transfer effectiveness of natural dye. This influences the sensitization effect, thus having a direct impact on the conversion efficiency of DSSC. Therefore, one of the ways to improve the photoelectric conversion efficiency is by controlling the temperature of dye extraction.

6.4 I-V & P-V characteristics

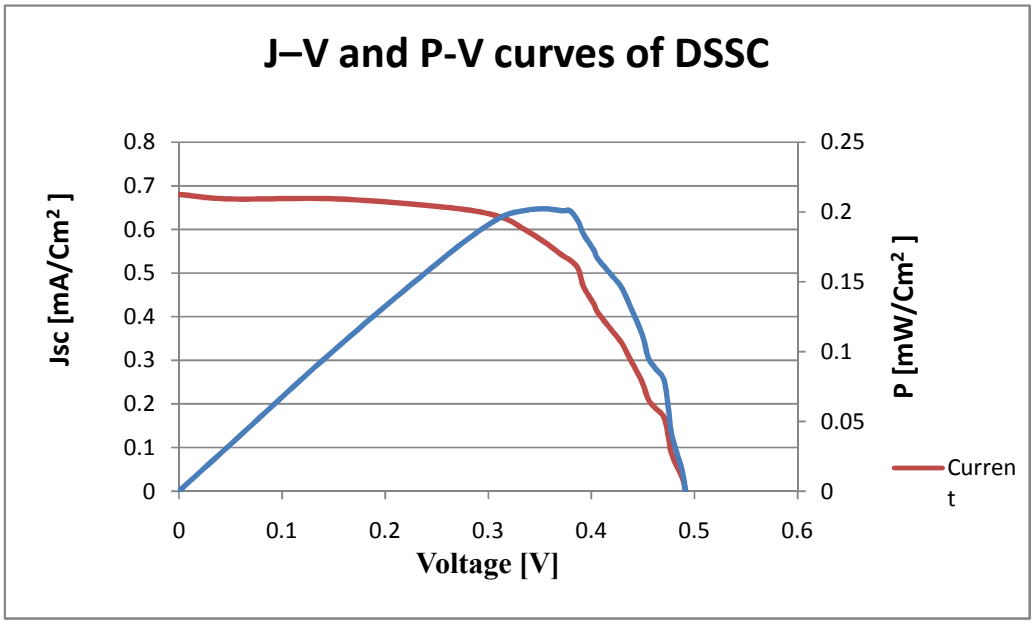

Fig. 6.5.J–V and P-V curves of Fe_2O_3dped TiO2 PhotoelectrodeDSSC for maximum efficiency of 0.20 % using tip of candle flame as a catalyst for counter electrode, film thickness of electrode is 20 µm and annealing temperaturewas 450 °C.

6.4.1 Discussion

A normal I-V curve has a smooth shape with three distinct voltage regions:

1. A slightly sloped region above 0 V

2. A steeply sloped region below Voc
3. A bend or 'knee' in the curve in the region of the maximum power point

The I-V (current-voltage) curve of a PV string (or module) describes its energy conversion capability at the existing conditions of irradiance (light level) and temperature. Conceptually, the curve represents the combinations of current and voltage at which the string could be operated or 'loaded', if the irradiance and cell temperature could be held constant. Figure 6.4 shows a typical I-V curve, the power-voltage or P-V curve that is computed from it, and key points on these curves.

Referring to Figure 6.4, the span of the I-V curve ranges from the short circuit current (Isc)
at zero volts, to zero current at the open circuit voltage (Voc). At the 'knee' of a normal I-V curve is the maximum power point (Imp, Vmp), the point at which the array generates maximum electrical power. In an operating PV system, one of the jobs of the inverter is to constantly adjust the load, seeking out the particular point on the I-V curve at which the array as a whole yields the greatest DC power.

At voltages well below Vmp, the flow of solar-generated electrical charge to the external load is relatively independent of output voltage. Near the knee of the curve, this behavior starts to change. As the voltage increases further, an increasing percentage of the charges recombine within the solar cells rather than flowing out through the load. At Voc, all of the charges recombine internally. The maximum power point, located at the knee of the curve, is the (I,V) point at which the product of current and voltage reaches its maximum value.

Any impairment that reduces the fill factor also reduces the output power by reducing Imp or Vmp or both. The I-V curve itself helps us identify the nature of these impairments. The effects of various losses(In dye , in electrolyte, in counter electrode preparation etc.) on the I-V curve are represented in Figure 6.4.

7 Chapter 7

7.1Conclusion

As a novel photovoltaic technology, dye-sensitized solar cells (DSSCs) have potential to compete with traditional solar cells. Materials such as TiO2 used in DSSCs are generally inexpensive,abundant and innocuous to the environment. Compared with silicon solar cells, they are insensitive to impurities in fabrication process, which accelerates a transition from research laboratory to mass production line. From the perspective of application, low weight and flexibility of DSSCs are desirable for the portable electronic device. It is found that DSSCs work better than silicon solar cells in the darker condition, for example, in the dawn and dusk, and also the overall efficiency is not seriously affected in the high temperature. In addition, the transparency and varied color of DSSCs could be utilized for decorative purposes like windows and sunroof. Up to now, such benefits have attracted considerable company investment and government funding. It is believed that with consistent efforts, DSSCs will be a reliable electrical power supplier in the future.

Natural pigments can be used as photosensitizers in DSSCs. However, the efficiency η is still by a factor of 3–4 lower than with synthetic dyes. But natural pigments are normally non-poisonous, can be disposed easily, and should be cheaper and more environmentally friendly than synthetic metal complexes. Therefore, natural dyes as light harvesting elements in DSSCs can contribute to a sustainable solution for the future energy production. Nature supplies a huge variety of putative structures for photosensitizers and combinations may enhance stability, efficiencies, and sustainability.

Dye sensitized cells are very tolerant to the effects of impurities because both light absorption and charge separation occur near the interface between two materials. The relative impurity tolerance and simplicity allows for easy, inexpensive scale-up to non-vacuum- and low-temperature-based high-volume manufacturing via continuous processes including screen-printing, spraying, pressing, or roll-to-roll production.

8 Chapter 8

8.1 Future Work Scope

In place of liquid electrolyte, solid or quasi-solid holeconductors can be employed, but the reduction in efficiency currently precludespracticalapplication.Thefirst, and still the most efficient electrolytes were liquid, so cell and module designs which prevented electrolyte leakage had to be developed to prevent evaporation. The stability and lifetime of DSC modules have thus reached appreciable values, and rapid improvements are being made.

High surface area electrodes can overcome both the recombination and the slow diffusion of the injected electron in the porous TiO2 layer.Tin dioxide (SnO2) is another attractive option having two main advantages over TiO2: high mobility, and large band gap. At room temperature 300 K, SnO2 electron mobility (ca. 100–200 cm2 V1 s1) was measured by Fonstad and Redikerwhich is three orders higher than that of TiO2 (ca. 0.1–1 cm2 V1 s1) . The larger band gap of SnO2 (3.8 eV), compared to TiO2 (3.2 eV), would create fewer oxidative holes in the valence band under ultraviolet illumination, thereby reducing the dye degradation rate and improving the long time stability of DSSCs. More positive band edge position facilitates electron injection from photoexcited dye molecules.

Moreover, it has been shown that the incorporation of carbon materials (e.g. carbon nanotubes, grapheme) in semiconductor photoanodes facilitates transport of photogenerated electrons to ultimately enhance the DSSC performance.So, there is scope to work with various carbon materials to improve photoanode efficiency .

Research on innovative dyes, for example, is expected to lead to considerable improvement in the cell's efficiency.

Besides enhancing the performance, how to lower materials cost is another important issue that needs to be addressed in the future work.

9 Chapter 9

Anonyms

1D	One-dimensional
3D	Three-dimensional
AC	Alternating current
AM	Air mass
at	Atomic
CB	Conduction Band
DC	Direct current
DSSCs	Dye-sensitized solar cells
EDTA	Ethylenediaminetetraacetic acid
EDX	Energy dispersive X-ray spectroscopy
EG	Ethylene glycol
EIS	Electrochemical impedance spectroscopy
FF	Fill factor
FRL	Fluoride-rich layer
FTO	Fluorine doped tin oxide
IPCE	Incident photon to current conversion efficiency
IS	Inner shell
I_{SC}	short-circuit current
I-V	current versus applied voltage
LED	Light-emitting diode
N719	cis-bis(isothiocyanato) bis (2,2-bipyridyl- bis(tetrabutylammonium)

NHE Normal hydrogen electrode

NT Nanotube

OCVD Open circuit voltage decay

OSOuter shell

RefReference

RTRoom temperature

SEMScanning electron microscopy

TCOTransparent conducting oxide

TEGtri-Ethylene glycol

TEMTransmission electron microscopy

TiTitanium

Fe Ferrum/ iron

ToF-SIMsTime of flight secondary ion mass spectrometry

VBValence Band

V_{OC}Open-circuit voltage

volVolume

Roman letters

A Absorbance/ Anatase XRD peak

d Thickness of the oxide

E Electric field strength

e Elementary charge

F Field strength

fc	Characteristic frequency minimum of the IMPS imaginary component
FF	Fill factor
fr	Characteristic frequency minimum of the IMVS imaginary component
I_{dark}	Dark diode current
I_{ph}	Constant photocurrent
Is	Diode saturation current
I_{SC}	short-circuit current
I_{shunt}	Shunting current
j	Current density
k	Boltzmann constant
m	Ideality factor
M	Molarity
P	Power
P_{in}	Incident solar power
R	Reflectance/ Rutile XRD peak
R_{ct}	Charge transfer resistance
R_{series}	Series resistance
R_{shunt}	Shunt resistance
t	Time
T	Absolute temperature
U	Applied potential
V	Voltage
V	Volume
V_{OC}	Open-circuit voltage

Greek letters

β	Temperature-dependent constants
ε	Molar extinction coefficient
η	Power conversion efficiency
η_{cc}	Charge collection efficiency
θ	X-ray scattering angle
λ	Wavelength
τc	Collection (transport) time
τr	Recombination time
φ	Quantum yields
Φ	Photon flux

Reference

[1] Renewable Energy, About Renewable Energy Technologies. (https://www.google.com/url?sa=t&rct=j&q=&esrc=s&source=web&cd=6&cad=rja&uact=8&ved=0ahUKEwjuveq6sL_KAhVLcY4KHWmhDcoQFghSMAU&url=http%3A%2F%2Fwww.renewableenergyworld.com%2Findex%2Ftech.html&usg=AFQjCNEkjQWfyFk9dN3MZwPRlTgqBEOOdA)

[2] About Thin Film. (http://www.google.com/patents/WO2013119550A1?cl=en)

[3] About Generation of Solar Cell. (http://org.ntnu.no/solarcells/pages/generations.php)

[4] Sol-gel Process. (http://www.twi-global.com/technical-knowledge/faqs/process-faqs/faq-what-is-sol-gel-processing/)

[5] CdTe Cell. (http://www.nrel.gov/pv/thinfilm.html)

[6] QDSC. (http://mbe.rcast.u-tokyo.ac.jp/index_eng.html)

[7] X. Chen and S. S. Mao, Chem. Rev. 2007, 107, 2891.

[8] S. D. Mo and W. Y. Ching, Phys Rev B 1995, 51, 13023.

[9] E. Halary-Wagner, F. Wagner and P. Hoffmann, J. Electrochem. Soc. 2004, 151, C571.

[10] C. Colbeau-Justin, M. Kunst and D. Huguenin, J. Mater. Sci. 2003, 38, 2429.

[11] T. Sumita, T. Yamaki, S. Yamamoto and A. Miyashita, Appl Surf Sci 2002, 200, 21.

[12] A. Shiga, A. Tsujiko, S. Yae and Y. Nakato, Bull. Chem. Soc. Jpn. 1998, 71, 2119.

[13] M. Takahashi, K. Tsukigi, T. Uchino and T. Yoko, Thin Solid Films 2001, 388, 231.

[14] P. Salvador, J. Appl. Phys. 1984, 55, 2977.

[15] Q. Shen, K. Katayama, T. Sawada, M. Yamaguchi, Y. Kumagai and T. Toyoda, Chem.

Phys. Lett. 2006, 419, 464.

[16] S. N. Habisreutinger, L. Schmidt-Mende and J. K. Stolarczyk, Angew. Chem. Int. Ed. 2013, 52, 7372.

[17] J. Li and N. Wu, Catalysis Science and Technology 2015, 5, 1360.

[18] Fujishima A and Honda K 1972 *Nature* **238** 37

[19] Grzmil B, Glen M, Kic B, Lubkowski K 2011 *Ind. Eng. Chem.Res.* **50** 6535

[20] Buchalska M, Kras G, Oszajca M, Łasocha W and Macyk W 2010 *J. Photochem. Photobiol. A: Chem.* **213** 158

[21] Newman M D, Stotland M and Ellis J I 2009 *J. Am. Acad. Dermatol.* **61** 685

[22] Zallen R and Moret M P 2006 *Solid State Commun.***137** 154

[23] Braun J H, Baidins A and Marganski R E 1992 *Prog. Org. Coat.* **20** 105

[24] Yang P, Zhao D, Margolese D I, Chmelka B F and Stucky G D 1988 *Nature* **396** 152

[25] Tian B, Liu X, Tu B, Yu C, Fan J, Wnang L, Xie S, Stucky G D and Zhao D 2003 *Nat. Mater.* **2** 159

[26] Regan B O and Gratzel M 1991 *Nature* **353** 737

[27] Nakade S, Saito Kubo Y W, Kitamura T, Wada Y and Yanagida S 2003 *J. Phys. Chem. B* **107** 8607

[28] Martinson A B F, Hamann T W, Pellin M J and Hupp J T 2008 *Chem. Eur. J.* **14** 4458

[29] Kim Y J, Lee M H, Kim H J, Lim G, Choi Y S, Park N G, Kim K and Lee W I 2009 *Adv. Mater.* **21** 3668

[30] Deanna C H, Alexander G A and Kimberly A G 2003 *J. Phys. Chem. B* **107** 4545

[31] A. Mishra, M. Fischer, P. Bäuerle **Metal-free organic dyes for dye-sensitized solar cells: from structure: property relationships to design rules** AngewChem Int Edit, 48 (2009), pp. 2474–2499

[32] G. Calogero, J. Yum, A. Sinopoli, G. Di Marco, M. Grätzel, M.K. Nazeeruddin **Anthocyanins and betalains as light-harvesting pigments for dye-sensitized solar cells** Sol. Energy, 86 (2012), pp. 1563–1575

[33] M. Kimura, H. Nomoto, N. Masaki, S. Mori

Dye molecules for simple co-sensitization process: fabrication of mixed-dye-sensitized solar cells

AngewChem Int Edit, 51 (2012), pp. 4371–4374

[34] K. Willinger, M. Thelakkat

Photosensitizers in solar energy conversion

T. Nyokong, V. Ahsen (Eds.), Photosensitizers in medicine, environment, and security, Springer, Netherlands (2012), pp. 527–617

[35]N.J. Cherepy, G.P. Smestad, M. Grätzel, J.Z. Zhang

Ultrafast electron injection: implications for a photoelectrochemical cell utilizing an anthocyanin dye-sensitized TiO2 nanocrystalline electrode

J PhysChem B, 101 (1997), pp. 9342–9351

[36] E. Galoppini

Linkers for anchoring sensitizers to semiconductor nanoparticles

CoordChem Rev, 248 (2004), pp. 1283–1297

[37] H. Imahori, T. Umeyama, S. Ito

Large π-aromatic molecules as potential sensitizers for highly efficient dye-sensitized solar cells

AccChem Res, 42 (2009), pp. 1809–1818

[38] A. Vittadini, A. Selloni, F.P. Rotzinger, M. Grätzel

Large π-aromatic molecules as potential sensitizers for highly efficient dye-sensitized solar cells

AccChem Res, 104 (2000), pp. 1300–1306

[39]K.E. Lee, M.A. Gomez, S. Elouatik, G.P. Demopoulos

Further understanding of the adsorption mechanism of N719 sensitizer on anatase TiO_2 films for DSSC applications using vibrational spectroscopy and confocal raman imaging

Langmuir, 26 (2010), pp. 9575–9583

[40]S. Ito, H. Miura, S. Uchida, M. Takata, K. Sumioka, P. Liska, *et al.*

High-conversion-efficiency organic dye-sensitized solar cells with a novel indoline dye

ChemCommun, 41 (2008), pp. 5194–5196

[41] W. Zhang, R. Zhu, B. Liu, S. Ramakrishna

High-performance hybrid solar cells employing metal-free organic dye modified TiO_2 as photoelectrode

Appl Energy, 90 (2012), pp. 305–308

[42] F.G. Gao, A.J. Bard, L.D. Kispert

Photocurrent generated on a carotenoid-sensitized TiO_2 nanocrystallinemesoporous electrode

J PhotochemPhotobiol A, 130 (2000), pp. 49–56

[43] Y. Eiji, M. Masaki, N. Naomi, H. Noritsugu, S. Masashi, K. Osamu

Utilization of natural carotenoids as photosensitizers for dye-sensitized solar cells

Sol. Energy, 81 (2007), pp. 512–516

[44] Y. Koyama, T. Miki, X.F. Wang, H. Nagae

Dye-sensitized solar cells based on the principles and materials of photosynthesis: mechanisms of suppression and enhancement of photocurrent and conversion efficiency

Int J MolSci, 10 (2009), pp. 4575–4622

[45] Y. Koyama, Y. Kakitani, H. Nagae

Mechanisms of suppression and enhancement of photocurrent/conversion efficiency in dye-sensitized solar-cells using carotenoid and chlorophyll derivatives as sensitizers

Molecules, 17 (2012), pp. 2188–2218

[46] X. Wang, Y. Koyama, H. Nagae, Y. Yamano, M. Ito, Y. Wada

Photocurrents of solar cells sensitized by aggregate-forming polyenes: enhancement due to suppression of singlet–triplet annihilation by lowering of dye concentration or light intensity

ChemPhysLett, 420 (2006), pp. 309–315

[47] X. Wang, R. Fujii, S. Ito, Y. Koyama, Y. Yamano, M. Ito, *et al.*

Dye-sensitized solar cells using retinoic acid and carotenoic acids: dependence of performance on the conjugation length and the dye concentration

ChemPhysLett, 416 (2005), pp. 1–6

[48] X. Wang, A. Matsuda, Y. Koyama, H. Nagae, S. Sasaki, H. Tamiaki, *et al.*

Effects of plant carotenoid spacers on the performance of a dye-sensitized solar cell using a chlorophyll derivative: enhancement of photocurrent determined by one electron-oxidation potential of each carotenoid

ChemPhysLett, 423 (2006), pp. 470–475

[49] S. Hao, J. Wu, Y. Huang, J. Lin

Natural dyes as photosensitizers for dye-sensitized solar cell

Sol Energy, 80 (2006), pp. 209–214

[50] M.R. Narayan

Review: dye sensitized solar cells based on natural photosensitizers

Renew Sustain Energy Rev, 16 (2012), pp. 208–215

[51] H. Zhou, L. Wu, Y. Gao, T. Ma

Dye-sensitized solar cells using 20 natural dyes as sensitizers

J PhotochemPhotobiol A, 219 (2011), pp. 188–194

[52] E.H. de Faria, A.L. Marçal, E.J. Nassar, K.J. Ciuffi, P.S. Calefi

Sol–gel TiO_2 thin films sensitized with the mulberry pigment cyanidin

Mater Res, 10 (2007), pp. 413–417

[53] K. Wongcharee, V. Meeyoo, S. Chavadej

Dye-sensitized solar cell using natural dyes extracted from rosella and blue pea flowers

Solar Energy Mater Solar Cells, 91 (2007), pp. 566–571

[54] G. Calogero, G. Di Marco, S. Cazzanti, S. Caramori, R. Argazzi, A. Di Carlo, *et al.*

Efficient dye-sensitized solar cells using red turnip and purple wild sicilian prickly pear fruits

Int J MolSci, 11 (2010), pp. 254–267

[55] W.H. Lai, Y.H. Su, L.G. Teoh, M.H. Hon

Commercial and natural dyes as photosensitizers for a water-based dye-sensitized solar cell loaded with gold nanoparticles

J PhotochemPhotobiol A, 195 (2008), pp. 307–313

[56] N.M. Gómez-Ortíz, I.A. Vázquez-Maldonado, A.R. Pérez-Espadas, G.J. Mena-Rejón, J.A. Azamar-Barrios, G. Oskam

Dye-sensitized solar cells with natural dyes extracted from achiote seeds

Solar Energy Mater Solar Cells, 94 (2010), pp. 40–44

[57] C.G. Garcia, A.S. Polo, N.Y. Murakami Iha

Fruit extracts and ruthenium polypyridinic dyes for sensitization of TiO_2 in photoelectrochemical solar cells

J PhotochemPhotobiol A, 160 (2003), pp. 87–91

[58] A.S. Polo, N.Y. Murakami Iha
Blue sensitizers for solar cells: natural dyes from Calafate and Jaboticaba
Solar Energy Mater Solar Cells, 90 (2006), pp. 1936–1944
[59] E. Yamazaki, M. Murayama, N. Nishikawa, N. Hashimoto, M. Shoyama, O. Kurita
Utilization of natural carotenoids as photosensitizers for dye-sensitized solar cells
Sol. Energy, 81 (2007), pp. 512–516
[60] G. Calogero, G.D. Marco
Red Sicilian orange and purple eggplant fruits as natural sensitizers for dye-sensitized solar cells
Solar Energy Mater Solar Cells, 92 (2008), pp. 1341–1346
[61] Henning A, Gunzburger G, Johr R, Rosenwaks Y, Bozic-Weber B, Housecroft CE, et al. Kelvin probe force microscopy of nanocrystalline TiO2 photoelectrodes. Beilstein J Nanotechnol 2013;4:418–28.
[62] N. Li, N. Pan, D. Li, S. Lin
Natural dye-sensitized solar cells based on highly ordered TiO_2 nanotube arrays
Int J Photoenergy, 2013 (2013), p. 5
[63] N.T.R.N. Kumara, P. Ekanayake, A. Lim, L.Y.C. Liew, M. Iskandar, L.C. Ming, *et al.*
Layered co-sensitization for enhancement of conversion efficiency of natural dye sensitized solar cells
J Alloys Compd, 581 (2013), pp. 186–191
[64] H. Kim, Y. Bin, S.N. Karthick, K.V. Hemalatha, C.J. Raj, S. Venkatesan, *et al.*
Natural dye extracted from *Rhododendron* species flowers as a photosensitizer in dye sensitized solar cell
Int J ElectrochemSci, 8 (2013), pp. 6734–6743
[65] B. O'Regan and M. Grätzel, **"A low-cost, high-efficiency solar cell based on dyesensitized colloidal TiO_2 films"**Naturr, vol. 353, No. 6346, pp. 737 – 740, (1991).
[66] Tsung-Wei Lin, Jun-Ren Lin, Sheng-You Tsai, Jing-Nang Lee, and Chen-Ching Ting, **"Absorption Spectra Analysis of Natural Dyes for Applications in Dye Sensitized Nano Solar Cells"**,
National Conference on Theoretical and Applied Mechanics, Vol, 96, pp, 21-22, (2007).
[67] P. Luo, H. Niu, G. Zheng, X. Bai, M. Zhang, W. Wang, **"From salmon pink to blue natural sensitizers for solar cells: Canna indica L., Salvia splendens, cowberry and**

Solanumnigrum L.", Spectrochim. Acta Part A Vol. 74 pp. 936–942, (2009)

[68] Huizhi Zhou, Liqiong*Wu*, YurongGao, Tingli Ma **" Dye-sensitized solar cells using 20 natural dyes as sensitizers"** Journal of Photochemistry and Photobiology A: Chemistry, Vol. 219, No. 2, pp.188–194 (2011)

[69] R. G. Gordon, **"Criteria for Choosing Transparent Conductors,"**MRS Bulletin, vol. 25, No.8, pp. 52-57, August (2000).

[70] Hoda Hafez, Zhang Lan, Qinghua Li, et alnovel **TiO_2nanorod/nanoparticle (NR/NP) bilayer electrode in the N719 dye-sensitized solar cells**

[71] C.B. Song et al. **DSSCusingTiO2 nanotube/nanoparticle (NT/NP) photoanodes and Cu2SnSe3 (CTSe) counter electrodes**.

Int. J. Electrochem. Sci., 9 **(2014)** 8090 - 8096

[72] Seulgi So et al. **Construction of DSSCs based on hierarchically structured single walled, self-organized TiO_2 layers**.

[73] Jiajie Fan et al. **Dye-sensitized solar cells (DSSCs) based on TiO_2nanosheets (TiO_2-NSs)/graphenenanocomposite films**.

[74] JiaopingCai et al. **titanium dioxide (TiO2) slurry formula for the fabrication of TiO2 photoanode for use in dye-sensitized solar cells (DSSCs).**

[75] T. Marinado, K. Nonomura, J. Nissfolk, M. K. Karlsson, D. P. Hagberg, L. Sun, S. Mori, and A. Hagfeldt,

How the Nature of Triphenylamine-Polyene Dyes in Dye-SensitizedSolar Cells Affects the Open-Circuit Voltage and Electron Lifetimes,

Langmuir, 2010, 26,2592

[76] National Renewable Energy Laboratory (2012), Reference Solar Spectral Irradiance: Air Mass 1.5, Retrieved September 01, 2012 from http://rredc.nrel.gov/solar/spectra/am1.5/

[77] M. Grätzel, ***Recent Advances in Sensitized Mesoscopic Solar Cells***, Acc. Chem. Res., 2009, 42 (11), 1788-1798.

[78] M. Planck, *AnP* 1901, 309, 553.

[79] C. J. Barbé, F. Arendse, P. Comte, M. Jirousek, F. Lenzmann, V. Shklover and M. Grätzel, *J. Am. Ceram. Soc.* 1997, 80, 3157.

[80] M. K. Nazeeruddin, A. Kay, I. Rodicio, R. Humphry-Baker, E. Müller, P. Liska, N. Vlachopoulos and M. Grätzel, *J. Am. Chem. Soc*. 1993, 115, 6382.

[81] K. Kalyanasundaram and M. Grätzel, *Coord. Chem. Rev.* 1998, 177, 347.

[82] B. O'Regan and M. Grätzel, *Nature 1991*, 353, 737.

[83] M. Grätzel, *Nature 2001, 414*, 338.

[84] A. Hagfeldt, G. Boschloo, L. Sun, L. Kloo and H. Pettersson, *Chem. Rev. 2010, 110,* 6595,

[85] M. Grätzel, *J. Photochem. Photobiol.C 2003, 4*, 145.

[86] S. Wenger in *Strategies to Optimizing Dye-Sensitized Solar Cells: Organic Sensitizers*, *Tandem Device Structures, and Numerical Device Modeling, Vol. doctoral dissertation*
ÉCOLE POLYTECHNIQUE FÉDÉRALE DE LAUSANNE, Switzerland, 2010.

[87] K. A. Emery and C. R. Osterwald*, SoCe 1986*, 17, 253.

[88] S. M. Sze, *Semiconductor Devices: Physics and Technology, 2nd Edition, John Wiley*
& Sons, Inc., 2001, p. 568 pp.

[89] C. J. Barbé, F. Arendse, P. Comte, M. Jirousek, F. Lenzmann, V. Shklover and M. Grätzel, *Nanocrystalline Titanium Oxide Electrodes for Photovoltaic Applications*, Journal of the American Ceramic Society, 1997, 80(12), 3157–3171.

[90] V. Shklover, M. K. Nazeeruddin, S. M. Zakeeruddin, C. Barbé, A. Kay, T. Haibach, W. Steurer, R. Hermann, H. U. Nissen, and M. Grätzel, *Structure of Nanocrystalline TiO_2 Powders and Precursor to Their Highly Efficient Photosensitizer*, Chem. Mater., 1997,9(2), 430–439.

[91] S. Nakade, M. Matsuda, S. Kambe, Y. Saito, T. Kitamura, T. Sakata, Y. Wada, H. Mori, and S. Yanagida, ***Dependence of TiO_2Nanoparticle Preparation Methods andAnnealing Temperature on the Efficiency of Dye-Sensitized Solar Cells***, J. Phys. Chem. B, 2002, 106 (39), 10004-10010.

[92] S. Nakade, Y. Saito, W. Kubo, T. Kitamura, Y. Wada, and S. Yanagida ,***Influence ofTiO_2 Nanoparticle Size on Electron Diffusion and Recombination in Dye-Sensitized TiO2 Solar Cells***, J. Phys. Chem. B 2003, 107, 8607-8611.

[93] M. K. Nazeeruddin, P. Péchy, T. Renouard, S. M. Zakeeruddin, R. Humphry-Baker, P. Comte, P. Liska, L. Cevey, E. Costa, V. Shklover, L. Spiccia, G. B. Deacon, C. A. Bignozzi, and M. Grätzel, ***Engineering of Efficient Panchromatic Sensitizers forNanocrystalline TiO_2-Based Solar Cells***, J. Am. Chem. Soc., 2001, 123(8), 1613-1624.

[94] M. Grätzel, *Conversion of sunlight to electric power by nanocrystalline dye-sensitizedsolar cells*, Journal of Photochemistry and Photobiology A: Chemistry, 2004, 164(1–3),3-14.

[95] S. Ito, M. K. Nazeeruddin, S. M. Zakeeruddin, P. P´echy, P. Comte, M. Gr¨atzel, T. Mizuno, A. Tanaka, and T. Koyanagi, *Study of Dye-Sensitized Solar Cells by ScanningElectron Micrograph Observation and Thickness Optimization of Porous TiO_2 Electrodes*,International J. Photoenergy, 2009, 2009, 517609.

[96] L. Meng, and C. Li, *Blocking Layer Effect on Dye-Sensitized Solar Cells Assembledwith TiO_2Nanorods Prepared by DC Reactive Magnetron Sputtering,* Nanoscience andNanotechnology Letters, 2011, 3(2), 181–185.

[97] P. J. Cameron and L. M. Peter, *Characterization of Titanium Dioxide Blocking Layersin Dye-Sensitized Nanocrystalline Solar Cells*, J. Phys. Chem. B, 2003, 107, 14394-14400.

[98] A. Burke, S. Ito, H. Snaith, U. Bach, J. Kwiatkowski, and M. Grätzel, *The Function of aTiO_2 Compact Layer in Dye-Sensitized Solar Cells Incorporating "Planar" Organic Dyes*,Nano Lett., 2008, 8(4), 977–981.

[99] S. Ito, T. N. Murakami, P. Comte, P. Liska, C. Grätzel, M. K. Nazeeruddin, M. Grätzel, ***Fabrication of thin film dye sensitized solar cells with solar to electric power conversion efficiency over 10%***, Thin Solid Films, 2008, 516(14), 4613–4619.

[100] H. Choi, C. Nahm, J. Kim, J. Moon, S. Nam, D. Jung, and B. Park, *The effect of $TiCl_4$-treated TiO_2 compact layer on the performance of dye-sensitized solar cell,* CurrentApplied Physics, 2012, 12(3), 737–741.

[101] O'Regan B, Grätzel M. Nature 1991;353:737.

[102] Kazmerski LL. J Electron SpectroscRelatPhenom 2006;150:105.

[103] Hoshikawa T, Ikebe T, Yamada M, Kikuchi R, Eguchi K. J PhotochemPhotobiol A 2006;184:78944.

[104] Xia J, Li F, Huang C, Zhai J, Jiang L. Solar energy mater. Solar Cells 2006;90:944.

[105] Hwang KJ, Jung SH, Park DW, Yoo SJ, Lee JW. CurrApplPhys 2010;10:S184.

[106] Chou CS, Guo MG, Liu KH, Chen YS.Appl Energy 2012;92:224.

[107] Lee JK, Jeong BH, Jang SI, Kim YG, Jang YW, Lee SB. J IndEngChem 2009;15:724.

[108] Singh J, Im J, Whitten JE, Soares JW, Steeves DM. ChemPhysLett 2010;497:196.

[109] Al-Kahlout A. **Thin Solid Films** 2012;520:1814.

[110] Wen X, Wang S, Ding Y, Wang ZL, Yang S. J PhysChem 2004;B109:215.

[111] Hwang KJ, Jung SH, Park DW, Yoo SJ, Lee JW. Curr. Appl. Phys 2010;10:S184.

[112] Carp O, Huisman C L, Reller A. Photoinduced reactivity of titanium dioxide. Prog in Solid State Chem, 2004, 32: 33–117

[113] Mor G K, Varghese O K, Paulose M, et al. **A review on highly ordered, vertically oriented TiO_2 nanotube arrays: Fabrication, material properties, and solar energy applications**. Solar Energy Mater Solar Cell, 2006, 90: 2011–2075

[114] Burda C, Lou Y, Chen X, et al. Enhanced nitrogen doping in TiO2 nanoparticles. Nano Lett, 2003, 3: 1049–1051.

[115] Szaciłowski K, Macyk W, Drzewiecka-Matuszek A, et al. **Bioinorganic photochemistry: Frontiers and mechanisms**. Chem Rev, 2005, 105: 2647–2694.

[116] Grätzel M, Howe R F. Electron paramagnetic resonance studies of doped TiO2 colloids. J PhysChem, 1990, 94: 2566–2572.

[117] Choi Y, Termin A, Hoffmann M R. The role of metal ion dopants in quantum-sized TiO2: Correlation between photoreactivity and charge carrier recombination dynamics. J PhysChem, 1994, 98: 13669–13679.

[118] Joshi M M, Labhsetwar N K, Mangrulkar P A, et al. Visible light induced photoreduction of methyl orange by N-doped mesoporoustitania. App Catal A General, 2009, 357: 26–33.

[119] Maruska H P, Ghosh A K. Transition-metal dopants for extending the response of titanatephotoelectrolysis anodes. Sol Energy Mater, 1979, 1: 237–247

[120] Gautron J, Lemasson P, Marucco J M. Correlation between the non-stoichiometry of titanium dioxide and its photoelectrochemical behaviour. Faraday Discuss ChemSoc, 1981, 70: 81–91

[121] Fox M A, Dulay M T. Heterogeneous photocatalysis. Chem Rev, 1995, 93: 341–357

[122] Xin B, Ren Z, Wang P, et al. **Study on the mechanisms of photoinduced carriers separation and recombination for Fe3+-TiO2 photocatalysts**. App Surf Sci, 2007, 253: 4390–4395

[123] Li R, Chen W, Wang W. Magnetoswitchable controlled photocatalytic system using ferromagnetic Fe-doped titanianorodsphotocatalysts with enhanced photoactivity. Sep PurifTechnol, 2009, 66: 171–176

[124] Periyasami V, Chinnathambi M, Chinnathambi S, et al. Photocatalyticactivity of iron doped nanocrystallinetitania for the oxidative degradation of 2,4,6-trichlorophenol. Catal Today, 2009, 141: 220–224